

DEVELOPMENT OF AN ELECTRONIC ATTACK (EA) SYSTEM
IN
MULTI-TARGET TRACKING

A THESIS SUBMITTED TO
THE GRADUATE SCHOOL OF NATURAL AND APPLIED SCIENCES
OF
MIDDLE EAST TECHNICAL UNIVERSITY

BY

ÖZLEM TÜRKÇÜ

IN PARTIAL FULFILLMENT OF THE REQUIREMENTS
FOR
THE DEGREE OF MASTER OF SCIENCE
IN
ELECTRICAL AND ELECTRONICS ENGINEERING

DECEMBER 2007

DEVELOPMENT OF AN ELECTRONIC ATTACK (EA) SYSTEM IN
MULTI-TARGET TRACKING

submitted by **ÖZLEM TÜRKÇÜ** in partial fulfilment of the requirements
for the degree of **Master of Science in Electrical and Electronics
Engineering Department, Middle East Technical University** by,

Prof. Dr. Canan Özgen _____
Dean, Graduate School of **Natural and Applied Sciences**

Prof. Dr. İsmet Erkmen _____
Head of Department, **Electrical and Electronics Engineering**

Prof. Dr. M. Kemal LEBLEBİCİOĞLU _____
Supervisor, **Electrical and Electronics Engineering Dept., METU**

Examining Committee Members:

Prof. Dr. Uğur HALICI _____
Electrical and Electronics Engineering Dept., METU

Prof. Dr. M. Kemal LEBLEBİCİOĞLU _____
Electrical and Electronics Engineering Dept., METU

Assoc. Prof. Dr. Yasemin Yardımcı ÇETİN _____
Informatics Institute, METU

Assoc. Prof. Dr. S. Gökhun TANYER _____
Institute Vise Person, TUBITAK-UEKAE

Assist. Prof. Dr. İlkey ULUSOY _____
Electrical and Electronics Engineering Dept., METU

Date: _____ 03.12.2007

I hereby declare that all information in this document has been obtained and presented in accordance with academic rules and ethical conduct. I also declare that, as required by these rules and conduct, I have fully cited and referenced all material and results that are not original to this work.

Name, Last name: TÜRKCÜ, Özlem

Signature:

ABSTRACT

DEVELOPMENT OF AN ELECTRONIC ATTACK (EA) SYSTEM IN MULTI-TARGET TRACKING

Türkçü, Özlem

M.Sc., Department of Electrics and Electronics Engineering

Supervisor: Prof. Dr. M. Kemal Leblebicioğlu

September 2007, 97 pages

In this study, an expert system based EA and tracking system is developed and the performances of these systems are optimized.

Tracking system consists of a monopulse tracking radar and a Multiple Hypothesis Tracking (MHT) algorithm. MHT is modelled as a measurement-oriented approach, which is capable of initiating tracks. As each measurement is received, probabilities are calculated for the hypotheses and target states are estimated using a Kalman filter.

Range Gate Pull-Off (RGPO) is selected as an EA technique to be developed because it is accepted to be the primary deception technique employed against tracking radar. Two modes of RGPO technique; linear and parabolic, according to time delay controller are modelled.

Genetic Algorithm (GA) Toolbox of MATLAB is used for the optimization of these systems over some predetermined scenarios. It is observed that the performance of the tracking radar system is improved significantly and successful tracking is achieved over all given scenarios, even for closely spaced targets. RGPO models are developed against this improved tracking performance and deception of tracking radar is succeeded for all given target models.

Keywords: Multiple Hypothesis Tracking, Range Gate Pull-Off, Optimization, Monopulse Target Tracking Radar, Genetic Algorithm.

ÖZ

ÇOKLU HEDEF İZLEMEDE ELEKTRONİK TAARRUZ (ET) SİSTEMİNİN GELİŞTİRİLMESİ

Türkçü, Özlem

Yüksek Lisans, Elektrik ve Elektronik Mühendisliği Bölümü

Tez Yöneticisi: Prof. Dr. M. Kemal Leblebicioğlu

Eylül 2007, 97 sayfa

Bu çalışmada, uzman sistem temelli elektronik taarruz sistemi ve izleme sistemi geliştirilmiş ve bu sistemlerin performansları eniyilenmiştir.

İzleme sistemi tek darbe izleme radarı ve Çoklu Hipotezle İzleme algoritmasını içermektedir. İz başlatabilme kabiliyetine sahip Çoklu Hipotezle İzleme algoritması, ölçüm yönlü yaklaşımla modellenir. Her bir ölçüm alındığında, hipotezlerin olasılıkları hesaplanır ve hedef durumları bir Kalman süzgeci kullanılarak tahmin edilir.

Menzil kapısı kaydırması, izleme radarlarına karşı kullanılan birincil aldatma tekniği kabul edildiği için geliştirilecek elektronik taarruz tekniği olarak seçilmiştir. Zaman geciktirme denetleyicisine göre doğrusal ve parabolik olmak üzere, iki menzil kapısı kaydırma modu modellenmiştir.

MATLAB Genetik Algoritma araç kutusu, bu sistemlerin verilen tüm senaryolar üzerinden eniyilenmesi için kullanılmıştır. İzleme radar sistemine ilişkin performans belirgin şekilde iyileştirilmiş ve yakın aralıklı hedefleri de içeren tüm senaryolarda başarılı izleme performansı elde edilmiştir. Menzil kapısı kaydırma modelleri, iyileştirilen izleme performansına karşı geliştirilmiş ve izleme radarının aldatması verilen tüm hedef modelleri için başarılı olmuştur.

Anahtar Kelimeler: Çoklu Hipotezle İzleme, Menzil Kapısı Kaydırma, Eniyileme, Tek Darbe Hedef İzleme Radarı, Genetik Algoritma.

To My Family

ACKNOWLEDGMENTS

It is a pleasure for me to express my sincere gratitude to my supervisor Prof. Dr. M. Kemal Leblebiciođlu for his guidance, advice, sensitivity, encouragements and sharing all his thoughts.

I would like to thank my colleagues from TUBITAK UEKAE, ILTAREN Research Group for their supports.

The technical assistance of Mr. M. Alper řahin is gratefully acknowledged.

I will also never forget to unending reliance, love and support of my family all the times.

Finally, I want to thank all my friends who are always by my side and helped me to keep myself away from hopelessness.

TABLE OF CONTENTS

ABSTRACT	iv
ÖZ.....	vi
ACKNOWLEDGMENTS	ix
TABLE OF CONTENTS	x
LIST OF TABLES.....	xii
LIST OF FIGURES.....	xiii
LIST OF ABBREVIATIONS.....	xv
CHAPTER	
1. INTRODUCTION	1
2. TARGET TRACKING RADAR.....	5
2.1 MONOPULSE THEORY.....	6
2.1.1 Class IA Type Monopulse.....	8
2.2 MONOPULSE RADAR MODEL.....	12
3. TRACKING FILTER	19
3.1 MULTIPLE HYPOTHESIS TRACKING.....	19
3.1.1 Measurement Conversion.....	22
3.1.2 Gating.....	24
3.1.3 Merging and Splitting a Cluster.....	25
3.1.4 Hypothesis Generation Technique	26
3.1.5 Hypothesis Probability Calculation.....	32
3.1.6 Combining.....	36
3.1.7 Pruning	37
3.1.8 Prediction and Filtering.....	38

4. ELECTRONIC ATTACK (EA) TECHNIQUES.....	40
4.1 EA TYPES.....	41
4.1.1 Active EA.....	41
4.1.2 Passive EA.....	47
4.2 EA MODEL.....	49
4.2.1 RGPO Model.....	50
5. OPTIMIZATION.....	52
5.1 PARAMETERS AND CONSTRAINTS.....	53
5.2 COST FUNCTION.....	57
5.3 OPTIMIZATION SCENARIOS.....	58
5.3.1 Multi-Target.....	58
5.3.2 Single-Target.....	74
5.4 THE GENETIC ALGORITHM.....	76
5.4.1 The Genetic Algorithm Toolbox.....	77
6. RESULTS & DISCUSSION.....	78
6.1 TRACKING RADAR SIMULATOR OPTIMIZATION.....	78
6.2 RGPO OPTIMIZATION.....	84
6.2.1 Linear RGPO.....	85
6.2.2 Parabolic RGPO.....	88
7. CONCLUSION.....	92
REFERENCES.....	95

LIST OF TABLES

Table 3-1 Hypotheses after the first scan processing for the first example.	27
Table 3-2 Hypotheses after the second scan processing for the first example.	28
Table 3-3 Hypotheses after the first scan processing for the second example.	29
Table 3-4 Hypotheses after the second scan processing for the second example.....	30
Table 5-1 Parameters of tracking radar.....	54
Table 5-2 Parameters of MHT.	55
Table 5-3 Parameters of RGPO.....	56
Table 5-4 Motion characteristics of target models in scenario 1.....	59
Table 5-5 Motion characteristics of target models in scenario 2.....	61
Table 5-6 Motion characteristics of target models in scenario 3.....	63
Table 5-7 Motion characteristics of target models in scenario 4.....	65
Table 5-8 Motion characteristics of target models in scenario 5.....	67
Table 5-9 Motion characteristics of target models in scenario 6.....	70
Table 5-10 Motion characteristics of target models in scenario 4.....	73
Table 5-11 Six target models motion characteristics.	75
Table 5-12 Settings of MATLAB GA tool parameters.....	77
Table 6-1 Optimized values of tracking radar simulator.	80
Table 6-2 Performances of tracking radar simulator with optimized values.	84
Table 6-3 Optimized values of linear RGPO.....	86
Table 6-4 Optimized values of parabolic RGPO.....	89

LIST OF FIGURES

Figure 1-1 STT system.	1
Figure 1-2 MTT system.....	2
Figure 2-1 Six different monopulse systems.	7
Figure 2-2 Monopulse antenna pattern for amplitude sensing.....	8
Figure 2-3 Block diagram of Class IA type monopulse.....	10
Figure 2-4 Monopulse radar model.....	12
Figure 2-5 Angles of target.	13
Figure 2-6 Split range gate.	16
Figure 3-1 Multiple Hypothesis Tracking approach overview.....	20
Figure 3-2 Flow chart of Multiple Hypothesis Tracking approach.	21
Figure 3-3 Hypothesis tree representation of the first example.....	28
Figure 3-4 Hypothesis tree representation of the second example.....	31
Figure 3-5 One cycle in the state estimation procedure of Kalman filter. ...	39
Figure 4-1 Range gate pull-off (RGPO).....	44
Figure 4-2 Cross polarization jamming of monopulse radar [22].....	46
Figure 4-3 Polarizations of chaff [23].....	48
Figure 4-4 Passive decoy.	49
Figure 4-5 Repeater pulse position for two modes.	50
Figure 5-1 Block diagram of simulation environment.....	52
Figure 5-2 The 3D path of target models in scenario 1.....	59
Figure 5-3 Target trajectories on two coordinates in scenario 1.....	60
Figure 5-4 The 3D path of target models in scenario 2.....	61

Figure 5-5 Target trajectories on the x coordinate in scenario 2.....	62
Figure 5-6 The 3D path of target models in scenario 3.....	63
Figure 5-7 Target trajectories on one coordinate in scenario 3.....	64
Figure 5-8 Difference of the two target trajectory on the y coordinate.	64
Figure 5-9 The 3D path of target models in scenario 4.....	66
Figure 5-10 Target trajectories on two coordinates in scenario 4.....	66
Figure 5-11 The 3D path of target models in scenario 5.....	68
Figure 5-12 Target trajectories on two coordinates in scenario 5.....	68
Figure 5-13 Target trajectories on the x coordinate in scenario 5.....	69
Figure 5-14 The 3D path of target models in scenario 6.....	70
Figure 5-15 Target trajectories on one coordinate in scenario 6.....	71
Figure 5-16 Difference of the two target trajectory on the y coordinate.	71
Figure 5-17 The 3D path of target models in scenario 7.....	74
Figure 6-1 Costs of each generation for tracking radar simulator.	79
Figure 6-2 Target and track trajectories on the x coordinate for scenario 2 (crossing targets).	82
Figure 6-3 Target and track trajectories on the y coordinate for scenario 4 (parallel targets).	82
Figure 6-4 Target and track trajectories on the y coordinate for scenario 6 (converging-diverging targets).	83
Figure 6-5 Costs of each generation for linear RGPO.....	85
Figure 6-6 Output of linear RGPO for target 1.	87
Figure 6-7 Output of linear RGPO for target 4.	88
Figure 6-8 Costs of each generation for parabolic RGPO.....	89
Figure 6-9 Output of parabolic RGPO for target 3.....	90
Figure 6-10 Output of parabolic RGPO for target 5.....	91

LIST OF ABBREVIATIONS

MTT	:	Multiple Target Tracking
STT	:	Single Target Tracking
MHT	:	Multiple Hypothesis Tracking
RF	:	Radio Frequency
IF	:	Intermediate Frequency
EA	:	Electronic Attack
ES	:	Electronic Support
EP	:	Electronic Protection
RGPO	:	Range Gate Pull-Off
VGPO	:	Velocity Gate Pull-Off
AGC	:	Automatic Gain Controller
PDA	:	Probabilistic Data Association
PDAF	:	Probabilistic Data Association Filter
JPDAF	:	Joint Probabilistic Data Association Filter
GA	:	Genetic Algorithm
NN	:	Nearest Neighborhood
KF	:	Kalman Filter
IMM	:	Interacting Multiple Model
CW	:	Continuous Wave
CV	:	Constant Velocity
DWNA	:	Discrete White Noise Acceleration

CHAPTER 1

INTRODUCTION

Multi-target tracking (MTT) is an essential requirement for both military and civilian radar applications. Unknown targets, false reports and electronic attacks are the difficulties of associating measurements with the appropriate tracks.

There is a fundamental difference between single-target tracking (STT) and MTT systems. Figure 1-1 [2], shows the elements of a STT system. As shown in the figure measurement error is direct input for tracking filter. However it is not the case of MTT system because of the necessity of complex data association.

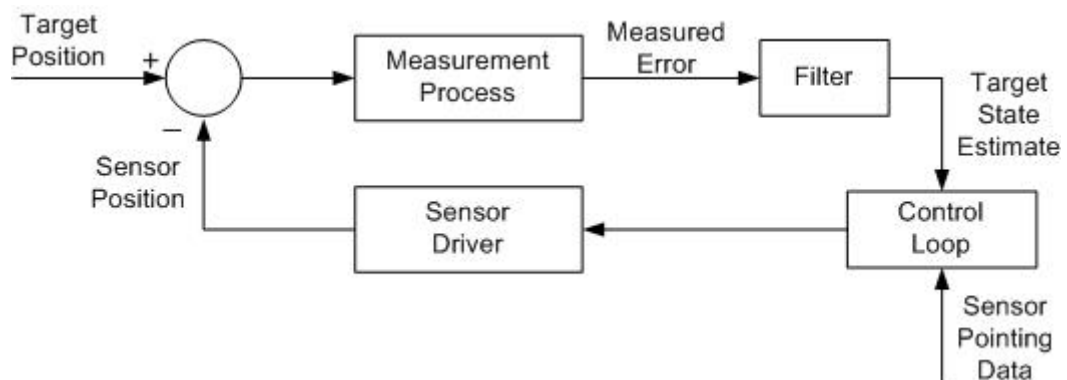


Figure 1-1 STT system.

Bar-Shalom and Tse developed the probabilistic data association filter (PDAF) for a single target with clutter measurements [6]. After developing PDAF, Bar-Shalom suggested a new technique to calculate the probability of each measurement originating from each target by extending this filter [7]. Thus multi target case is also enclosed. Typical functional elements of a simple MTT system [2] are given in Figure 1-2.

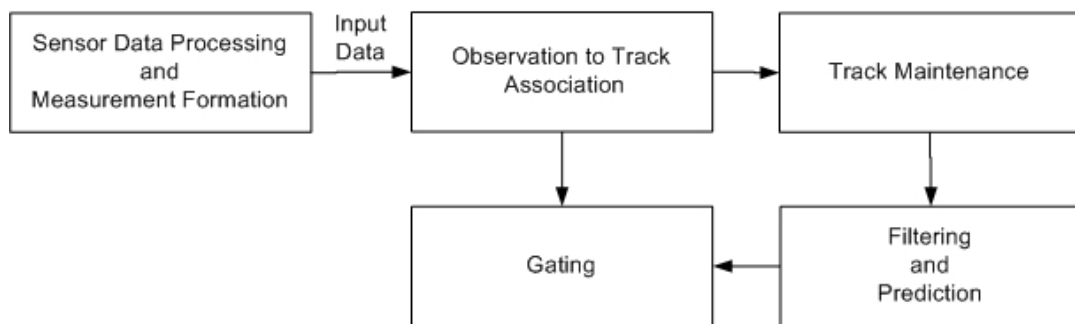


Figure 1-2 MTT system.

In a MTT system data association job - assigning measurements to tracks rapidly - is a fundamental problem to be solved. Due to its simplicity, nearest neighbourhood (NN) correlation is often used. However, it has limitations and shows poor performance in the case of closely spaced targets. Therefore, more complicated algorithms like probabilistic data association (PDA), interacting multiple model joint probabilistic data association (IMMJPDA) and MHT approaches are required. PDA is known often to cause miss tracking of closely space targets since it ignores the interference of other targets [24]. The main disadvantages of the other two approaches are mainly the requirements of considerable amount of computation and memory. Continuous advances in computer technology ease the utilization of these algorithms. When all these approaches are

compared, MHT is accepted to be superior to IMMJPDA and also to perform better than NN [17]. MHT is widely accepted to be the most successful data association algorithm in the target-dense and clutter-dense environments [2]. In this work, MHT is implemented for its advantages mentioned above.

MHT is developed by Reid [1]. It is defined as a measurement-oriented approach. This approach appears simpler than track-oriented approach for consideration of the track initiation requirement. In MHT as each measurement is received, probabilities are calculated for the hypotheses and target states are estimated using a Kalman filter.

Although, MHT is the most successful tracking algorithm, Electronic Attack (EA) still presents a greater challenge to target tracking compared to clutter and missed detections. The basic purpose of EA is to introduce signals into an enemy's receiver, which degrade the performance of that system so that it is unable to perform its intended mission [22]. Therefore many works have focused on the development of the efficient tracking algorithms and/or track radar system in the presence of EA [13, 14 and 26]. However, there are limited publications in the field of the performance improvement of EA systems. Success of EA techniques depends on both tracking system incapability's and parameters of EA techniques applied. Therefore, the main purpose of this thesis is to develop an EA model against a successful tracking system.

In this study tracking radar simulator that consists of a monopulse tracking radar and MHT tracker, is improved. Also the optimization of its

parameters is performed for achieving best tracking capability in absence of EA. Furthermore EA model is developed to have improved effectiveness against this tracking system.

In this thesis, target tracking radar with monopulse theory and processing signals for the monopulse model are explained in Chapter 2. In Chapter 3, MHT is described in details and each step of MHT logic with possible solutions is examined. In Chapter 4, types of EA techniques and also RGPO models are given. Problem variables, cost function construction, multi and single target scenarios are described in Chapter 5. Moreover, the Genetic Algorithm is explained as the optimization tool to be utilized. Results obtained by optimization of tracking radar simulator and RGPO models are discussed in Chapter 6. Finally, the conclusion of thesis is given in Chapter 7.

CHAPTER 2

TARGET TRACKING RADAR

A tracking radar system measures the coordinates of a target and provides one or more of the following:

- 1) Range by the elapsed time between transmission of the signal and reception of the return signal
- 2) Rate of change of range by measurement of Doppler shift
- 3) Azimuth and elevation angle by use of directive antenna patterns.

There are numerous features that can be used in classifications of radars [10]:

- Active or passive radar: Depending on the nature and location of the source of electromagnetic radiation.
- Short range, horizon or over-horizon radar: Depending on maximum effective range.
- Sequential lobbing, conical-scan or monopulse: Depending on the number of channels used to determine angular coordinates.
- Monostatic or multistatic radar: Depending on the positions of transmitting and receiving antennas.

The sequential lobbing and conical scan tracking radars require the train of echo pulses, must contain no amplitude modulation components other than the modulation produced by scanning in order to extract the accurate angle error signal. The tracking accuracy might be reduced if the frequency of the fluctuations were near the sequential lobbing rate or conical-scan frequency. In monopulse, angle error information can be obtained with only single pulse therefore; pulse-to-pulse amplitude fluctuations of the echo signal have no effect on tracking accuracy.

In this thesis, active-monostatic monopulse target tracking radar model [4] is utilized. The detailed explanation of monopulse theory and monopulse radar structure is given in [4] and will only be reviewed in this chapter.

2.1 MONOPULSE THEORY

D. R. Rhodes gives the general theory of monopulse based on the three postulates in [11] as follows:

- *Monopulse angle information appears in the form of a ratio: Angle information is extracted by comparing pairs of received signals and monopulse system will be a function of only the angle of arrival.*
- *The sensing ratio for a positive angle of arrival is the inverse of the ratio for an equal negative angle: Angle output function is symmetric on the boresight.*
- *The angle output function is an odd, real function of the angle of arrival: Angle output has odd symmetry about the bore sight direction and it is a real function of angle of arrival.*

Operation of a monopulse system defined by the three postulates can also be explained analytically as three transformations: Angle sensing, ratio conversion and angle detection. First transformation is the formation of the complex angle-sensing ratio. The angle-sensing ratio can be converted by a transformation into any other forms of sensing ratio satisfying the monopulse postulates. Finally, it is transformed into the angle detection function whose real part is odd and continuous with continuous derivatives.

Monopulse systems use either pure amplitude sensing or pure phase sensing. D. R. Rhodes identified three classes of monopulse by the terms amplitude, phase and sum-and-difference according to the type of angle detection. If angle sensor and angle detector types are considered, six different monopulse systems could be formed as showed in Figure 2-1.

Type of Angle Detector \ Type of Angle Sensor	Amplitude (A)	Phase (P)
Sum and Difference (class I)	IA	IP
Amplitude (class II)	IIA	IIP
Phase (class III)	IIIA	IIIP

Figure 2-1 Six different monopulse systems.

Since the application of the thesis on all radar types are beyond the scope of the work, only Class IA type monopulse radar is studied. Further information of all these six forms is available in [4] and [11].

2.1.1 Class IA Type Monopulse

An amplitude sensing sensor operates depending on the facts that far-field amplitude pattern of an antenna decreases when the scattering target move away from the boresight axis of an antenna [4]. In the amplitude-sensing sensor, two overlapping beams are formed with an offset of squint angle (Figure 2-2) to obtain the angular error in one coordinate. When the target is offset by an angle from the boresight axis, the signal received through the upper beam is less amplitude than the signal received through the lower beam. The amplitude of this difference signal ratio indicates angle of arrival.

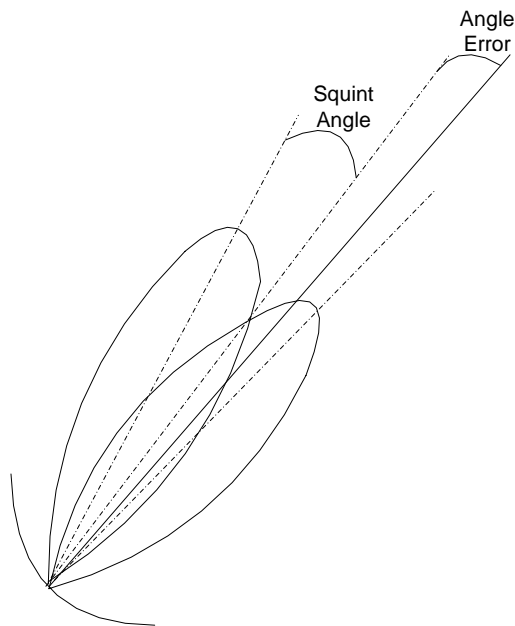


Figure 2-2 Monopulse antenna pattern for amplitude sensing.

The signals at the output of the amplitude sensing antenna for one-plane have the following form:

$$\begin{aligned}
 E(t) &= E_m e^{j\omega_{RF}t} \\
 E_1(t, \theta) &= E(t) F_1(\theta), \\
 E_2(t, \theta) &= E(t) F_2(\theta)
 \end{aligned}
 \tag{2-1}$$

where $E(t)$ is the target echo at the antenna, E_m is the received target echo voltage, E_1 and E_2 are the complex form of received target echo at each channel, F_1 and F_2 are the far-field amplitude pattern at the target angle and θ with respect to boresight axis.

A passive device performs subtraction and adding operations in RF (Radio Frequency) band for producing the sum signal, $\Sigma(\theta)$ and the difference signal, $\Delta(\theta)$ with the input from amplitude sensing antenna. The resulting signals are given below:

$$\begin{aligned}
 \Sigma(\theta) &= \frac{1}{\sqrt{2}} (E_1(t, \theta) + E_2(t, \theta)) \\
 &= \frac{1}{\sqrt{2}} E_m (F_1(\theta) + F_2(\theta)) e^{j\omega_{RF}t}
 \end{aligned}
 \tag{2-2}$$

$$\begin{aligned}
 \Delta(\theta) &= \frac{1}{\sqrt{2}} (E_1(t, \theta) - E_2(t, \theta)) \\
 &= \frac{1}{\sqrt{2}} E_m (F_1(\theta) - F_2(\theta)) e^{j\omega_{RF}t}
 \end{aligned}
 \tag{2-3}$$

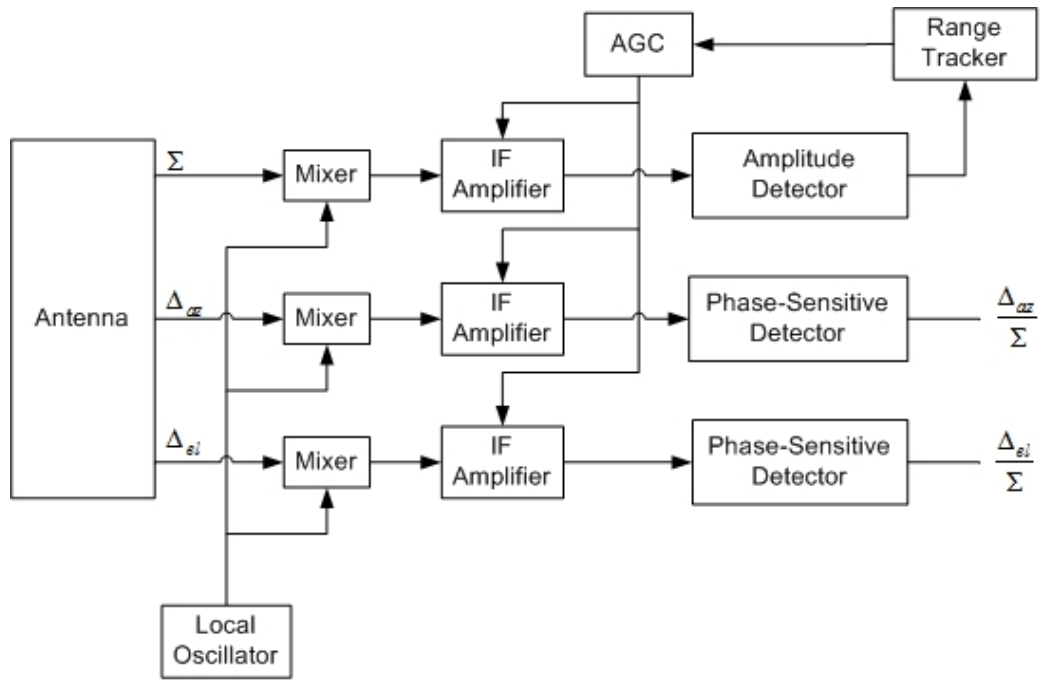


Figure 2-3 Block diagram of Class IA type monopulse.

After RF to IF (Intermediate Frequency) conversion, the signals in the sum and difference channels are passed through IF amplifier with the AGC feedback, showed in Figure 2-3, and the resultant signals at each channel with a phase shift $\Delta\varphi$, between channels are given as:

$$\begin{aligned}\Sigma(\theta) &= e^{j(\omega_{IF}t + \Delta\varphi)} \\ \Delta(\theta) &= \frac{k_d}{k_s} \left(\frac{F_1(\theta) - F_2(\theta)}{F_1(\theta) + F_2(\theta)} \right) e^{j\omega_{IF}t}\end{aligned}\tag{2-4}$$

where k_s and k_d are the IF amplifier gain of sum and difference channel. The output of the IF amplifier is given directly to the phase detector, which will produce the error signal, $\frac{\Delta}{\Sigma}(\theta)$ as

$$\frac{\Delta}{\Sigma}(\theta) = K_{PD} \frac{k_d}{k_s} \left(\frac{F_1(\theta) - F_2(\theta)}{F_1(\theta) + F_2(\theta)} \right) \cos(\Delta\varphi) \quad (2-5)$$

where K_{PD} is the phase detector gain.

Equation (2-5) can be simplified if the far-field amplitude patterns of amplitude sensing angle sensor are written as a function of non-squinted antenna pattern as

$$\begin{aligned} F_1(\theta) &= F(\gamma - \theta) \\ F_2(\theta) &= F(\gamma + \theta) \end{aligned} \quad (2-6)$$

where $F_1(\theta)$ and $F_2(\theta)$ are the far-field amplitude patterns of monopulse antenna, F is the far-field amplitude patterns of non-squinted beam, γ is the squint angle.

From the Taylor series expansion of F at $\theta = 0$ the far-field amplitude patterns can be rewritten as

$$\begin{aligned} F_1(\theta) &= F(\gamma - \theta) = F(\gamma)(1 + \nu\theta) \\ F_2(\theta) &= F(\gamma + \theta) = F(\gamma)(1 - \nu\theta) \end{aligned} \quad (2-7)$$

where

$$\nu = \left. \frac{dF}{d\theta} \right|_{\theta=0} \quad (2-8)$$

Using the relation given in equation (2-5) and (2-7), the phase detector output after low pass filtering can be rewritten as follows:

$$\begin{aligned}
\frac{\Delta}{\Sigma}(\theta) &= K_{PD} \frac{k_d}{k_s} \left(\frac{F_1(\theta) - F_2(\theta)}{F_1(\theta) + F_2(\theta)} \right) \cos(\Delta\varphi) \\
&= K_{PD} \frac{k_d}{k_s} \left(\frac{F(\gamma - \theta) - F(\gamma + \theta)}{F(\gamma - \theta) + F(\gamma + \theta)} \right) \cos(\Delta\varphi) \\
&= K_{PD} \frac{k_d}{k_s} \left(\frac{F(\gamma)(1 + \nu\theta) - F(\gamma)(1 - \nu\theta)}{F(\gamma)(1 + \nu\theta) + F(\gamma)(1 - \nu\theta)} \right) \cos(\Delta\varphi) \\
&= K_{PD} \frac{k_d}{k_s} \left(\frac{2\nu\theta F(\gamma)}{2F(\gamma)} \right) \cos(\Delta\varphi) \\
&= K_{PD} \frac{k_d}{k_s} \nu\theta \cos(\Delta\varphi)
\end{aligned} \tag{2-9}$$

2.2 MONOPULSE RADAR MODEL

In this section monopulse radar model is examined according to the signal processing.

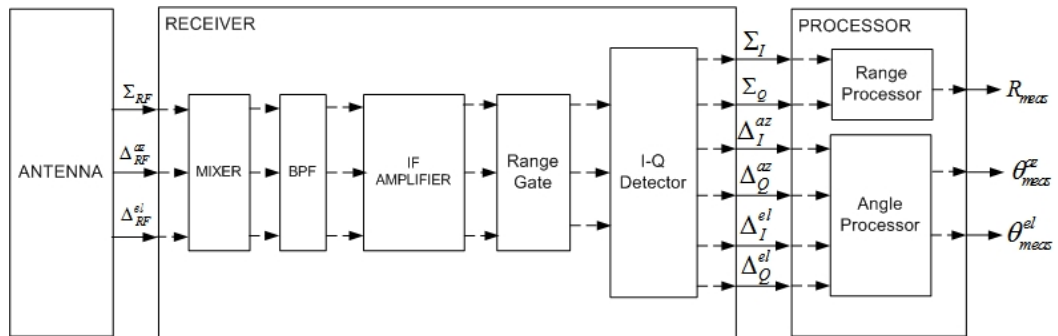


Figure 2-4 Monopulse radar model.

Planar phase array antenna is used to produce summation and difference of the target echo signals due to the advantages of simultaneous tracking of multiple targets using electronic scanning multiple arrays. A planar array consists of antenna elements arranged to line in a plane. The elements are equal spacing and their centers are contained within a rectangular area.

The antenna pattern of the rectangular planar array antenna at the target point I is the summation of the far-field amplitude patterns of all elements at that point. The target point located ϕ degrees off bore sight in the azimuth plane and θ degrees off bore sight in the elevation plane (Figure 2-5) forms the radiation pattern of a planar array antenna with $N \times M$ elements is given by:

$$F(\phi, \theta) = \sum_{n=0}^{N-1} \sum_{m=0}^{M-1} \left[\left(F_i^{nm}(\phi, \theta) a_{nm} e^{j b_{nm}} \right) e^{j \psi_{nm}(\phi, \theta)} \right] \quad (2-10)$$

where $F_i^{nm}(\phi, \theta)$ is the individual element pattern of the element at n^{th} row and m^{th} column of the rectangular grid, a_{nm} and b_{nm} are the amplitude and phases of the element, $\psi_{nm}(\phi, \theta)$ is the phase shift of the signal, transmitted from the array element at n^{th} row and m^{th} column of the rectangular grid, with respect to the center of the array aperture at the target point [20].

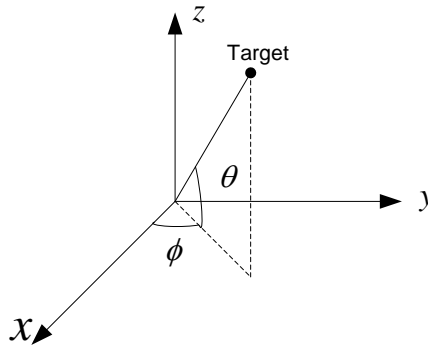


Figure 2-5 Angles of target.

In a rectangular planar array, lying on the xz plane, the phase shift $\psi_{nm}(\phi, \theta)$ in the far field region can be calculated as follows:

$$\psi_{nm}(\phi, \theta) = \frac{2\pi}{\lambda} \left(\vec{k}(\phi, \theta) \cdot \vec{r}_{nm} \right) \quad (2-11)$$

where $\vec{k}(\phi, \theta)$ is the direction vector of the target echo signal and \vec{r}_{nm} is the array element displacement vector which is placed at n^{th} row and m^{th} column [20] and $'.'$ denotes the dot product of two vectors.

Then the sum and difference signals (output of the antenna in Figure 2-4) at each channel provided by amplitude sensing type angle sensor can be written as:

$$\begin{aligned}\Sigma_{RF} &= \left[E_m(t) \cos[(w_{RF} - w_d)t] F_{sum}(\phi, \theta) \right] p\left(t - \frac{2R}{c}\right) + w_{\Sigma}(t), \\ \Delta_{RF}^{az} &= \left[E_m(t) \cos[(w_{RF} - w_d)t] F_{diffAz}(\phi, \theta) \right] p\left(t - \frac{2R}{c}\right) + w_{\Delta}^{az}(t), \\ \Delta_{RF}^{el} &= \left[E_m(t) \cos[(w_{RF} - w_d)t] F_{diffEl}(\phi, \theta) \right] p\left(t - \frac{2R}{c}\right) + w_{\Delta}^{el}(t)\end{aligned}\quad (2-12)$$

where $w_{RF} = 2\pi f_{RF}$, $w_d = 2\pi f_d$, f_{RF} is the radar carrier frequency, f_d is the Doppler shift at the returned signal due to velocity of the target, $p(t)$ is the transmitted pulse shape and w_{Σ} , w_{Δ}^{az} and w_{Δ}^{el} are the additive white Gaussian noise in each channel, $E_m(t) = \sqrt{2P_r(t)}$ and $P_r(t)$ can be calculated with the following equation:

$$P_r(t) = \frac{P_t G^2 \lambda^2 \sigma(t)}{(4\pi)^3 R(t)^4 L_{total}(t)} F_{sum}^2(\phi, \theta) \quad (2-13)$$

where P_t is the transmitter peak power, G is the gain of the antenna, λ is the wavelength of the carrier, $\sigma(t)$ is the radar cross section of the target at time t , $R(t)$ is the range between radar and target at time t and $L_{total}(t)$ is the total loss at the received signal at time .

The loss term $L_{total}(t)$ is the summation of the atmospheric attenuation loss ($L_a(t)$), transmission line loss ($L_{tr}(t)$) and the antenna loss ($L_{ant}(t)$) as follows:

$$L_{Tot} = L_a(t) + L_r(t) + L_{ant}(t) \quad (2-14)$$

In receiver stage, firstly RF signal is down converted to IF signal and then filtered at the band pass filter. Then the each channel signal is amplified by IF amplifier. The resultant is as follows,

$$\begin{aligned} \Sigma_{IF} &= k_{IF}^{sum} \left(\left[E_m(t) \cos[(w_{IF} - w_d)t] F_{sum}(\phi, \theta) \right] p\left(t - \frac{2R}{c}\right) + n_\Sigma(t) \right), \\ \Delta_{IF}^{az} &= k_{IF}^{diffAz} \left(\left[E_m(t) \cos[(w_{IF} - w_d)t] F_{diffAz}(\phi, \theta) \right] p\left(t - \frac{2R}{c}\right) + n_\Delta^{az}(t) \right), \\ \Delta_{IF}^{el} &= k_{IF}^{diffEl} \left(\left[E_m(t) \cos[(w_{IF} - w_d)t] F_{diffEl}(\phi, \theta) \right] p\left(t - \frac{2R}{c}\right) + n_\Delta^{el}(t) \right) \end{aligned} \quad (2-15)$$

where $w_{IF} = 2\pi f_{IF}$, f_{IF} is the IF frequency, k_{IF}^{sum} , k_{IF}^{diffAz} and k_{IF}^{diffEl} are the amplifier gains in the IF stage, $n_\Sigma(t)$, $n_\Delta^{az}(t)$ and $n_\Delta^{el}(t)$ are the filtered noise (i.e. narrow band noise) corresponding to each channel.

The Gaussian noise becomes band pass noise after applying the band pass filter. It has the appearance of a random amplitude modulation of carrier whose phase also varies randomly in time with representing as follows [12],

$$\begin{aligned} n(t) &= r(t) \cos(w_{IF}t + \varphi(t)) \\ &= r(t) (\cos(w_{IF}t) \cos(\varphi(t)) - \sin(w_{IF}t) \sin(\varphi(t))) \\ &= n_I(t) \cos(w_{IF}t) - n_Q(t) \sin(w_{IF}t) \end{aligned} \quad (2-16)$$

where $n(t)$ is the filtered noise with noise power, N can be calculated by the equation (2-17), n_I and n_Q are the in-phase and quadrature components of the filtered noise.

$$N = \frac{kT_n B_n}{2} \quad (2-17)$$

where T_n is the system noise temperature and B_n is the bandwidth of the band-pass noise.

As shown in Figure 2-4, targets at other ranges should be excluded by split range gate as shown in Figure 2-6. The range gate is positioned at the tracking filter target state estimation and the range gate width is predetermined by the optimization. Signals which will be written in the equations after this step are represented as the outputs of range gates for each channel.

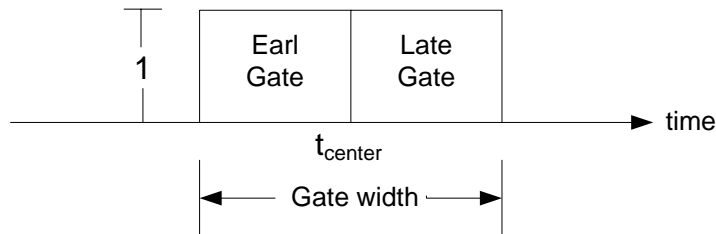


Figure 2-6 Split range gate.

The last block of receiver stage is I-Q detector. It provides in phase and quadrature components of the base band sum and difference signals to the monopulse processor. After down conversion of the IF signals by a low pass filter whose characteristics is “matched” to the transmitted pulse, I-Q detector is assumed to sample the signals. Each sample point is referred to as a range bin whose width is equal to the width of the pulse in the receiver model. The outputs of the I-Q detector are given as follows:

$$\begin{aligned}
\Sigma_I(k) &= \Sigma_I(t) \sum \delta(t - kT_s), \\
\Sigma_Q(k) &= \Sigma_Q(t) \sum \delta(t - kT_s), \\
\Delta_I^{az}(k) &= \Delta_I^{az}(t) \sum \delta(t - kT_s), \\
\Delta_Q^{az}(k) &= \Delta_Q^{az}(t) \sum \delta(t - kT_s), \\
\Delta_I^{el}(k) &= \Delta_I^{el}(t) \sum \delta(t - kT_s), \\
\Delta_Q^{el}(k) &= \Delta_Q^{el}(t) \sum \delta(t - kT_s)
\end{aligned} \tag{2-18}$$

where

$$\begin{aligned}
\Sigma_I(t) &= k_{IF}^{sum} \left(E_m(t) \cos(w_d t) F_{sum}(\phi, \theta_r^{el}) g(t - \frac{2R}{c}) + n_I^{sum}(t) \right), \\
\Sigma_Q(t) &= k_{IF}^{sum} \left(E_m(t) \sin(w_d t) F_{sum}(\phi, \theta) g(t - \frac{2R}{c}) + n_Q^{sum}(t) \right), \\
\Delta_I^{az}(t) &= k_{IF}^{az} \left(E_m(t) \cos(w_d t) F_{diffAz}(\phi, \theta) g(t - \frac{2R}{c}) + n_I^{diffAz}(t) \right), \\
\Delta_Q^{az}(t) &= k_{IF}^{az} \left(E_m(t) \sin(w_d t) F_{diffAz}(\phi, \theta) g(t - \frac{2R}{c}) + n_Q^{diffAz}(t) \right), \\
\Delta_I^{el}(t) &= k_{IF}^{el} \left(E_m(t) \cos(w_d t) F_{diffEl}(\phi, \theta) g(t - \frac{2R}{c}) + n_I^{diffEl}(t) \right), \\
\Delta_Q^{el}(t) &= k_{IF}^{el} \left(E_m(t) \sin(w_d t) F_{diffEl}(\phi, \theta) g(t - \frac{2R}{c}) + n_Q^{diffEl}(t) \right)
\end{aligned} \tag{2-19}$$

and T_s is the sampling period and $g(t)$ is the matched filter output of the transmitted pulse.

The processor block, last part of monopulse radar shown in Figure 2-4, detects the target and then calculates the target position from the output of the I-Q detector. The value of each range bins sum signal compares with the threshold. The range bin that satisfies the inequality (2-20) is the bin where target echo exists.

$$abs(\Sigma_I(k_b) + j\Sigma_Q(k_b)) \geq V_{th} \tag{2-20}$$

where k_b is at the bin in the range gate.

After determining range bins of targets, range and angle error values are calculated with the following equations,

$$\hat{r} = \frac{\sum_{i=1}^N (T_{pw} k_i - t_{left}) \frac{c}{2} |\Sigma_I(k_i) + j\Sigma_Q(k_i)|}{\sum_{i=1}^N |\Sigma_I(k_i) + j\Sigma_Q(k_i)|},$$

$$\hat{\phi} = \frac{1}{k_{az}} \frac{\sum_{i=1}^N \text{Re} \left\{ \frac{\Delta_{az}(k_i)}{\Sigma(k_i)} \right\}}{N} = \frac{1}{k_{az}} \frac{\sum_{i=1}^N \frac{\Sigma_I(k_i)\Delta_I^{az} + \Sigma_Q(k_i)\Delta_Q^{az}}{(\Sigma_I(k_i))^2 + (\Sigma_Q(k_i))^2}}{N}, \quad (2-21)$$

$$\hat{\theta} = \frac{1}{k_{el}} \frac{\sum_{i=1}^N \text{Re} \left\{ \frac{\Delta_{el}(k_i)}{\Sigma(k_i)} \right\}}{N} = \frac{1}{k_{el}} \frac{\sum_{i=1}^N \frac{\Sigma_I(k_i)\Delta_I^{el} + \Sigma_Q(k_i)\Delta_Q^{el}}{(\Sigma_I(k_i))^2 + (\Sigma_Q(k_i))^2}}{N}$$

where \hat{r} is the range error, $\hat{\phi}$ is the azimuth angle error and $\hat{\theta}$ is the elevation angle error, N is the number of detection in the range gate, T_{pw} is the pulse width and also the range bin length, t_{left} is early range gate in time, c is the speed of light, k_{az} and k_{el} are the error slopes. As a last step, the target position is calculated by the monopole processor in (2-22),

$$\begin{aligned} R_{Meas} &= \hat{r} + \frac{c}{2} t_{center}, \\ \phi_{Meas} &= \hat{\phi} + \phi_{Antenna}, \\ \theta_{Meas} &= \hat{\theta} + \theta_{Antenna} \end{aligned} \quad (2-22)$$

where R_{Meas} , ϕ_{Meas} and θ_{Meas} are the measured position, $\phi_{Antenna}$ and $\theta_{Antenna}$ are the direction of the boresight of the antenna, t_{center} is the center of the range gate.

Angle sensor, input for the radar receiver is given in (2-12), and the I-Q detector output can be computed as in (2-17). This procedure completes the measurement of the target position.

CHAPTER 3

TRACKING FILTER

Highly effective target tracking algorithms should be used in multi-target tracking (MTT) because of the necessity to detect and track targets in clutter with numerous false detections and missed detections. Furthermore the tracking algorithm should solve data association problem rapidly, especially for closely spaced or crossing targets. A technique that is known to be the best approach for providing the ability to handle the problem of data association in MTT is Multiple Hypothesis Tracking (MHT). In this chapter MHT algorithm is examined with possible alternative solutions at each time step, in details.

3.1 MULTIPLE HYPOTHESIS TRACKING

Reid [1] developed a complete approach utilizing the probabilities of the various data association hypothesis, multi-scan correlation and clustering features.

The overview of MHT approach is represented in Figure 3-1. When measurement input is received, gating is done to avoid generation of

unlikely hypotheses. Once track and hypothesis formation are completed, hypothesis evaluation is performed with track probability calculation to limit the number of hypotheses. Finally, track states are updated with a Kalman filter and the procedure repeats itself.

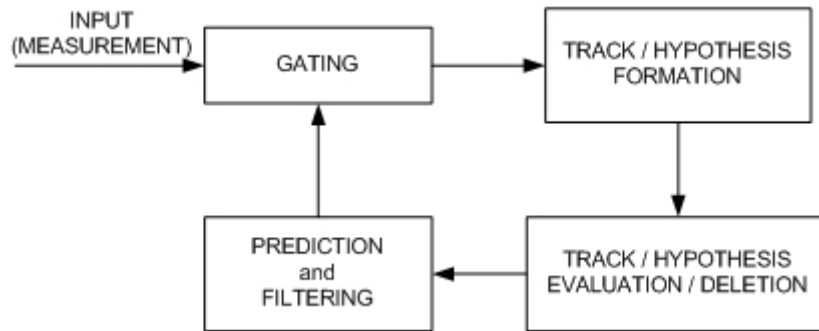


Figure 3-1 Multiple Hypothesis Tracking approach overview.

High-level flow chart of MHT approach used in this study is illustrated in Figure 3-2. As new measurements are received, they are gated with existing tracks. If the gates of tracks within more than one cluster enclose same measurements, the clusters are to be merged. Also new clusters are formed for the measurements that do not fall within the gates of tracks in existing clusters. When all the measurements have been processed, clusters may be split if it is possible. Then the formation of tracks and hypotheses begins for each cluster. Combining and pruning methods provide to limit the number of hypotheses. Finally, after all tracks are filtered for the prediction of the next scan, empty clusters are deleted and this cycle repeats itself. The details of all steps of MHT logic will be presented in the following sections.

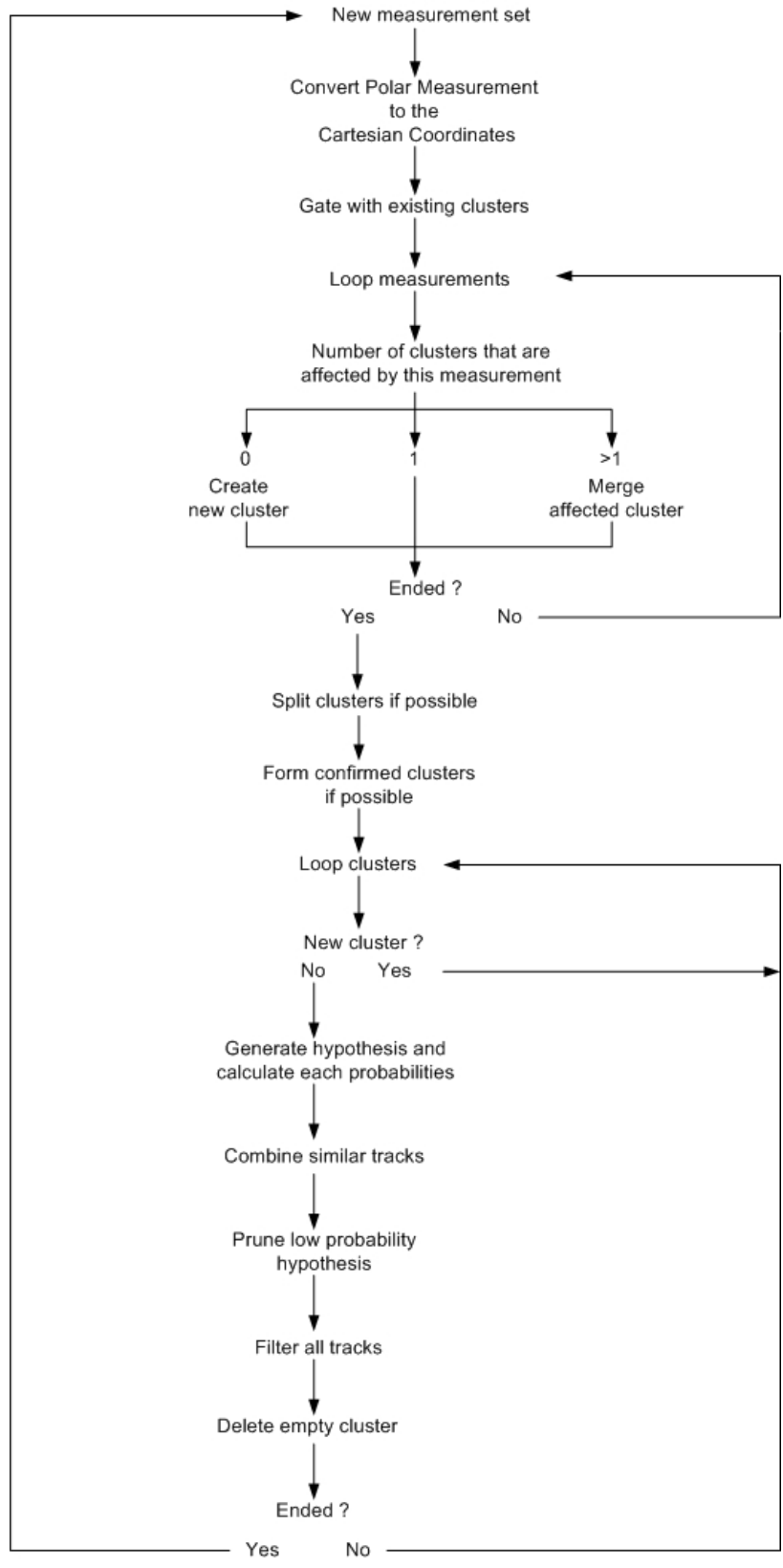


Figure 3-2 Flow chart of Multiple Hypothesis Tracking approach.

3.1.1 Measurement Conversion

Kalman filter uses an input in the form of Cartesian coordinate but the tracking radar produces polar measurements, so these polar measurements should be converted before processing. Measurements can be converted by using “standard coordinate conversion” if the inequalities given in equations (3-1) and (3-2) are satisfied [21]. Practically all systems satisfy the inequalities so we can use the standard coordinate conversion explained below,

$$\frac{r_m \sigma_\theta^2}{4\sigma_r} + \frac{r_m \sigma_\phi^2}{2\sigma_r} < 0.26 \quad (3-1)$$

$$\frac{\sigma_\theta^2 (2 - \sigma_\phi^2)}{8\sigma_\phi} < 0.27 \quad (3-2)$$

where σ_r^2 and σ_θ^2 are variance of error in range and azimuth, r_m is range measurement.

Polar measurements are transformed to the cartesian coordinates by the standard coordinate conversion given in (3-3),

$$\begin{aligned} x_m &= r_m \cos \phi_m \cos \theta_m \\ y_m &= r_m \cos \phi_m \sin \theta_m \\ z_m &= r_m \sin \phi_m \end{aligned} \quad (3-3)$$

where x_m , y_m and z_m are converted measurement in Cartesian coordinate, θ_m and ϕ_m are azimuth and elevation measurement.

The measurement covariance matrix must be recalculated for each measurement. Therefore, error statistics should be approximated by taking the first order terms of a Taylor series expansion of errors given in (3-4),

$$\begin{aligned}
x_e &= x_m - x = r_m \cos \phi_m \cos \theta_m - r \cos \phi \cos \theta \\
y_e &= y_m - y = r_m \cos \phi_m \sin \theta_m - r \cos \phi \sin \theta \\
z_e &= z_m - z = r_m \sin \phi_m - r \sin \phi
\end{aligned} \tag{3-4}$$

where x_e , y_e and z_e are errors in each Cartesian coordinates, r , θ and ϕ are the true target range, azimuth and elevation.

The output of the Taylor series expansion is given as [19]:

$$\begin{aligned}
x_e &= r_m \cos \phi_m \cos \theta_m - (r_m - r_e) \cos(\phi_m - \phi_e) \cos(\theta_m - \theta_e) \\
&= r_e (\cos \phi_m \cos \theta_m + \theta_e \cos \phi_m \sin \theta_m + \phi_e \sin \phi_m \cos \theta_m + \theta_e \phi_e \sin \phi_m \sin \theta_m) \\
&\quad - r_m (\theta_e \cos \phi_m \sin \theta_m + \phi_e \sin \phi_m \cos \theta_m + \theta_e \phi_e \sin \phi_m \sin \theta_m) \\
y_e &= r_m \cos \phi_m \sin \theta_m - (r_m - r_e) \cos(\phi_m - \phi_e) \sin(\theta_m - \theta_e) \\
&= r_e (\cos \phi_m \sin \theta_m - \theta_e \cos \phi_m \cos \theta_m + \phi_e \sin \phi_m \sin \theta_m - \theta_e \phi_e \sin \phi_m \cos \theta_m) \\
&\quad + r_m (\theta_e \cos \phi_m \cos \theta_m - \phi_e \sin \phi_m \sin \theta_m + \theta_e \phi_e \sin \phi_m \cos \theta_m) \\
z_e &= r_m \sin \phi_m - (r_m - r_e) \sin(\phi_m - \phi_e) \\
&= r_e (\sin \phi_m - \phi_e \cos \phi_m) + r_m \phi_e \cos \phi_m
\end{aligned} \tag{3-5}$$

Then, the elements of the measurement covariance matrix [19] are given in (3-6).

$$\begin{aligned}
R_{11} &= \text{var}(x_e | r_m, \theta_m, \phi_m) \\
&= r_m^2 (\sigma_\theta^2 \sigma_\phi^2 \sin^2 \theta_m \sin^2 \phi_m + \sigma_\theta^2 \cos^2 \phi_m \sin^2 \theta_m + \sigma_\phi^2 \cos^2 \theta_m \sin^2 \phi_m) \\
&\quad + \sigma_r^2 \left(\sigma_\theta^2 \sigma_\phi^2 \sin^2 \theta_m \sin^2 \phi_m + \sigma_\theta^2 \cos^2 \phi_m \sin^2 \theta_m + \right. \\
&\quad \left. \sigma_\phi^2 \cos^2 \theta_m \sin^2 \phi_m + \cos^2 \phi_m \sin^2 \theta_m \right) \\
R_{12} &= \text{var}(x_e, y_e | r_m, \theta_m, \phi_m) \\
&= -r_m^2 \sin \theta_m \cos \theta_m (-\sigma_\phi^2 \sin^2 \phi_m + \sigma_\theta^2 \sigma_\phi^2 \sin^2 \phi_m + \sigma_\theta^2 \cos^2 \phi_m) \\
&\quad + \sigma_r^2 \sin \theta_m \cos \theta_m (\sigma_\phi^2 \sin^2 \phi_m - \sigma_\theta^2 \sigma_\phi^2 \sin^2 \phi_m - \sigma_\theta^2 \cos^2 \phi_m + \cos^2 \phi_m) \\
R_{13} &= \text{var}(x_e, z_e | r_m, \theta_m, \phi_m) \\
&= \sin \phi_m \cos \phi_m \cos \theta_m (\sigma_r^2 - r_m^2 \sigma_\phi^2 - \sigma_r^2 \sigma_\phi^2) \\
R_{22} &= \text{var}(y_e | r_m, \theta_m, \phi_m) \\
&= r_m^2 (\sigma_\theta^2 \sigma_\phi^2 \cos^2 \theta_m \sin^2 \phi_m + \sigma_\theta^2 \cos^2 \phi_m \cos^2 \theta_m + \sigma_\phi^2 \sin^2 \theta_m \sin^2 \phi_m) \\
&\quad + \sigma_r^2 \left(\sigma_\theta^2 \sigma_\phi^2 \cos^2 \theta_m \sin^2 \phi_m + \sigma_\theta^2 \cos^2 \phi_m \cos^2 \theta_m + \right. \\
&\quad \left. \sigma_\phi^2 \sin^2 \theta_m \sin^2 \phi_m + \cos^2 \phi_m \sin^2 \theta_m \right) \\
R_{23} &= \text{var}(y_e, z_e | r_m, \theta_m, \phi_m) \\
&= \sin \phi_m \cos \phi_m \sin \theta_m (\sigma_r^2 - r_m^2 \sigma_\phi^2 - \sigma_r^2 \sigma_\phi^2) \\
R_{33} &= \text{var}(z_e | r_m, \theta_m, \phi_m) \\
&= r_m^2 \sigma_\phi^2 \cos^2 \phi_m + \sigma_r^2 (\sin^2 \phi_m + \sigma_\phi^2 \cos^2 \phi_m) \\
R_{21} &= R_{12} \\
R_{31} &= R_{13} \\
R_{32} &= R_{23}
\end{aligned} \tag{3-6}$$

where σ_r^2 , σ_θ^2 and σ_ϕ^2 are the variance of error in range, azimuth and elevation measurements, respectively.

3.1.2 Gating

A gate is a region formed around a track position for eliminating unlikely measurement to track association. There are two types of gates in order to be used before and after filter initialization. Rectangular prism, which is

defined by equation (3-7), is the first type of gate. It is used for tentative tracks.

$$Wrec = \begin{bmatrix} 2 \times (V_{x\max} \times T + \sqrt{R_x}) \\ 2 \times (V_{y\max} \times T + \sqrt{R_y}) \\ 2 \times (V_{z\max} \times T + \sqrt{R_z}) \end{bmatrix} \quad (3-7)$$

where $V_{x\max}$, $V_{y\max}$ and $V_{z\max}$ are the maximum expected velocity of the target in x, y and z direction, T is the update period of radar, R_x , R_y and R_z are the measurement noise variances defined for each axis.

After the filter initialization, predicted value of the measurement $\tilde{z}(k+1|z)$ and the associated covariance $S(k+1)$ has been known. Under this assumption, the true measurement conditioned on the past is normally (Gaussian) distributed with its probability density function given by (3-8),

$$p[z(k+1|k)|Z^k] = N[z(k+1); \tilde{z}(k+1|k), S(k+1)] \quad (3-8)$$

The true measurement will be in the region given by the equation (3-9) with probability determined by the gate threshold γ which is obtained from tables of the chi-square distributions [5].

$$V(k+1, \gamma) = \left\{ z : [z - \tilde{z}(k+1|k)]^T S(k+1)^{-1} [z - \tilde{z}(k+1|k)] < \gamma \right\} \quad (3-9)$$

3.1.3 Merging and Splitting a Cluster

Clusters are collections of hypotheses and associated tracks that are connected by common measurements. If the entire set of hypotheses can be divided into sets of independent clusters, instead of one large tracking

problem, a number of smaller tracking problems can be solved independently.

A new cluster is formed for each measurement that does not fall within the gate of any tracks in existing clusters. If a measurement falls within the gates of more than one cluster, then those clusters are merged into a “super cluster” [1]. The number of hypotheses in the new super cluster is the product of the number of hypotheses in the prior clusters and the probabilities of super cluster hypotheses are the products of the prior probabilities. All tracks of merged clusters are copied to the super cluster.

Cluster splitting procedure does not have specific rules like cluster merging. Clusters having more than one measurement should be split, if its tracks are associated with only one measurement. In another words, clusters should be split if its measurements do not have common tracks.

3.1.4 Hypothesis Generation Technique

Track-oriented and measurement-oriented are the two types of hypothesis generation approach. Track-oriented approach computes the hypotheses using the newly updated tracks after each scan of data are received [3]. It does not keep hypotheses from scan to scan. In the measurement-oriented approach, every possible hypothesis is listed for each measurement. Although both approaches are almost similar, measurement-oriented approach appears simpler considering track initiation requirement. This thesis focuses on the measurement-oriented approach, which is also the Reid’s original method.

Hypotheses are represented in a matrix form where the columns are measurements, the rows are hypotheses and the elements are tracks [8]. In the hypothesis matrix, a measurement may be correlated with a false alarm, with an existing track, or with the starting of a new track. Before associating a measurement to an existing track, a set of conditions must be satisfied. Firstly, the measurement must lie within the validation region of the track. Secondly, each track cannot be associated to more than one measurement per scan. The representation of hypothesis matrix with two measurements at two scan is illustrated with an example. Measurements are denoted as $z_i(k)$ (i^{th} measurement received on scan k). It is assumed that $z_1(1)$ is not used to update an existing track. Therefore, there are two alternatives of this measurement; false target (0) and new track (1), as shown in Table 3-1.

Table 3-1 Hypotheses after the first scan processing for the first example.

Hypothesis	$z_1(1)$
1	0
2	1

When a measurement $z_1(2)$ received on the next scan is considered, five hypotheses given in Table 3-2 are formed.

Table 3-2 Hypotheses after the second scan processing for the first example.

Hypothesis	$z_1(1)$	$z_1(2)$
1	0	0
2	1	0
3	1	1(2)
4	0	3
5	1	3

First, measurement is always declared as a false target (0) so previous hypotheses are continued with 0. Next, measurement correlates with existing tracks if the validation region condition is satisfied. In the third hypothesis, the track number is the previous track number and the numbers in the parentheses are given after the measurement is assigned. Finally, measurement starts a new track and two more hypotheses are created.

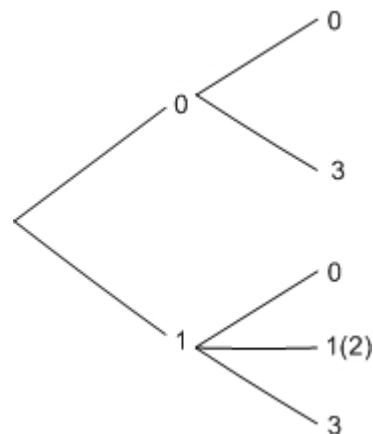


Figure 3-3 Hypothesis tree representation of the first example.

Another example is given to explain the hypothesis matrix in which both of the scans contain two measurements. When the first measurement $z_1(1)$ is

received, there are two hypotheses which are false target (0) and new track (1). After the second measurement $z_2(1)$ is received, first hypothesis retain their previous number and continue with a false target. Next, since one target produces no more than one measurement per scan, no associations with existing track 1 is allowed. Therefore, new track must be formed and two more hypotheses are created as shown in Table 3-3.

Table 3-3 Hypotheses after the first scan processing for the second example.

Hypothesis	$z_1(1)$	$z_2(1)$
1	0	0
2	1	0
3	1	2
4	0	2

As soon as the measurement of second scan is received, it is allowed to be a false target. Next, assuming that the validation regions of the tracks 1 and 2 are satisfied, four more hypotheses are formed linking $z_1(2)$ with track 1 and 2. Finally, hypotheses associated with the new track option are formed. Same procedure is applied for the second measurement of second scan $z_2(2)$. As a result, the hypothesis matrix in Table 3-4 and the hypothesis tree in Figure 3-4 have been formed.

Since identical tracks will appear in more than one hypothesis, track numbers of hypotheses should be stored to avoid inefficient computation of the same track for each hypothesis, as shown in the hypothesis tree representation in Figure 3-4.

Table 3-4 Hypotheses after the second scan processing for the second example.

Hypothesis	z1(1)	z2(1)	z1(2)	z2(2)
1	0	0	0	0
2	1	0	0	0
3	1	2	0	0
4	0	2	0	0
5	1	3	1(3)	0
6	1	2	1(3)	0
7	0	2	2(4)	0
8	1	2	2(4)	0
9	0	0	5	0
10	1	0	5	0
11	0	2	5	0
12	1	2	5	1(6)
13	1	0	0	1(6)
14	1	2	0	1(6)
15	1	2	2(4)	1(6)
16	1	0	5	1(6)
17	1	2	5	2(7)
18	0	2	0	2(7)
19	1	2	0	2(7)
20	1	2	1(3)	2(7)
21	0	2	5	2(7)
22	1	2	5	8
23	0	0	0	8
24	1	0	0	8
25	0	2	0	8
26	1	2	0	8
27	1	0	1(3)	8
28	1	2	1(3)	8
29	0	2	2(4)	8
30	1	2	2(4)	8
31	0	0	5	8
32	1	0	5	8
33	0	2	5	8
34	1	2	5	8

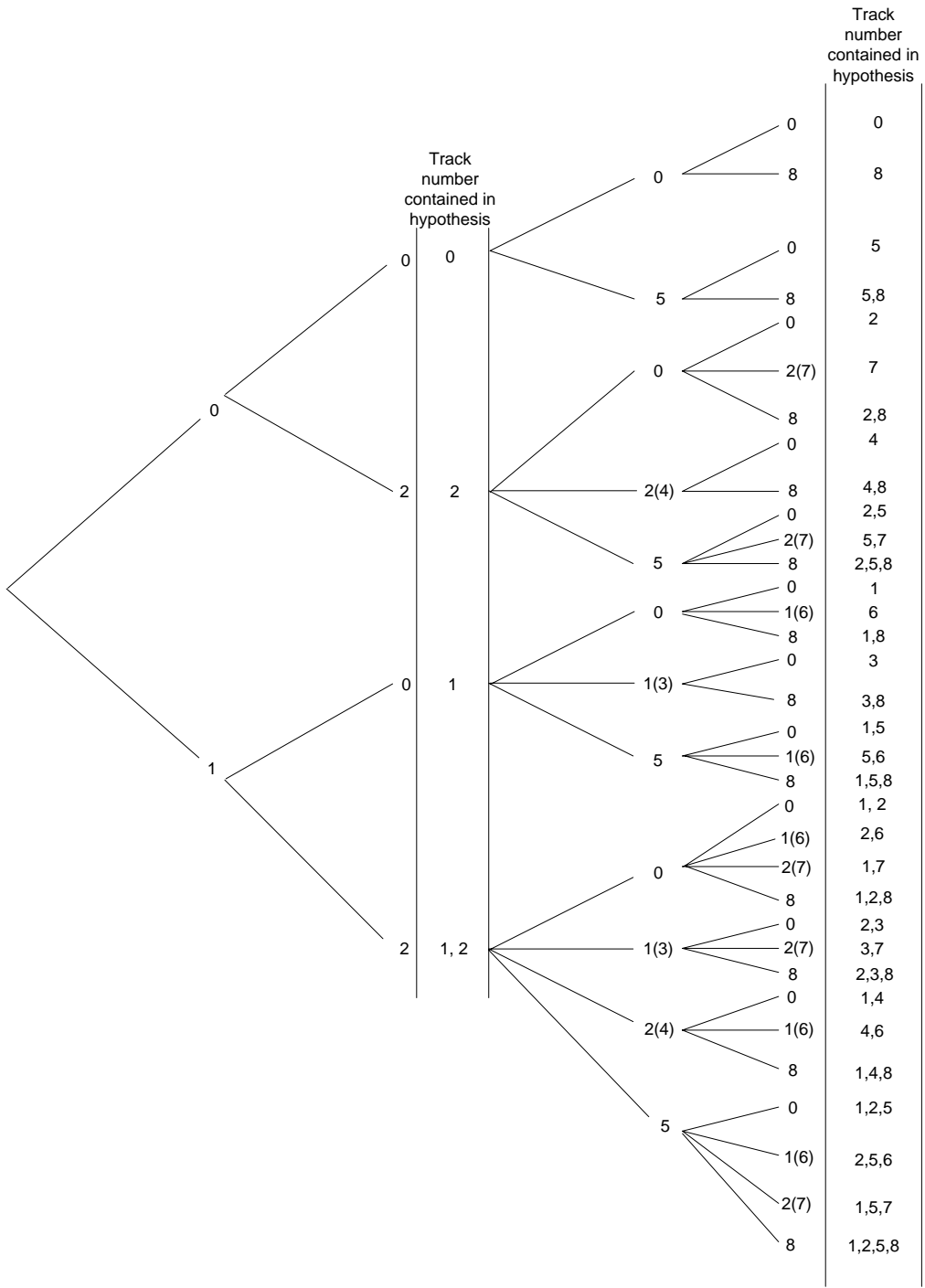


Figure 3-4 Hypothesis tree representation of the second example.

3.1.5 Hypothesis Probability Calculation

The derivation of the probability of each hypothesis given by Reid [1] is summarized in this section.

The probability of the hypothesis Ω_i^k , given measurements before the time step k is defined as,

$$P_i^k = P(\Omega_i^k | Z^k) \quad (3-10)$$

Recursive relationship for P_i^k by use of Bayes' equation is written by,

$$\begin{aligned} P(\Omega_i^k | Z^k) &= P(\Omega_g^{k-1}, \psi_h | Z^k) \\ &= \frac{1}{c} P(Z(k) | \Omega_g^{k-1}, \psi_h) P(\psi_h | \Omega_g^{k-1}) P(\Omega_g^{k-1}) \end{aligned} \quad (3-11)$$

where Ω_g^{k-1} is the prior hypothesis, ψ_h is the association hypothesis for the current data set and c is the normalization factor.

$P(\Omega_g^{k-1})$ represents the probability of a parent global hypothesis and therefore it is already known from the previous iteration.

The first term on the right hand side of equation (3-11), $P(Z(k) | \Omega_g^{k-1}, \psi_h)$, is the likelihood of the measurements $Z(k)$ and is evaluated by:

$$P(Z(k) | \Omega_g^{k-1}, \psi_h) = \begin{cases} \prod_{i=1}^{M_k} \frac{1}{V} & \text{if the } i^{\text{th}} \text{ measurement is from clutter or a new target} \\ \prod_{i=1}^{M_k} N(Z_i - H\bar{x}, B) & \text{if the measurement from a target whose} \\ & \text{existence is implied by the prior hypothesis } \Omega_g^{k-1} \end{cases} \quad (3-12)$$

where V is the volume of the region covered by the radar, $N(\bar{x}, P)$ is the normal distribution, \bar{x} and B are the mean and covariance of the target estimate for the prior hypothesis Ω_g^{k-1} .

Finally, the second term of the equation (3-11) is the probability of the current data association hypothesis, ψ_h given the prior hypothesis Ω_g^{k-1} . Each ψ_h associates each measurement including the information of *Number, Configuration and Assignment*.

Number: $N_{FT}(h)$, $N_{DT}(h)$ and $N_{NT}(h)$ are the number of measurements associated with the false target, prior targets and new targets respectively.

Configuration: It shows the measurements, which are from false targets, previously known as targets or new targets.

Assignment: It shows the specific source of each measurement assigned from some previously known target.

In addition, Ω_g^{k-1} includes information of the number of previously known targets $N_{TGT}(g)$ within the coverage area of the radar. However, only $N_{DT}(h)$ of these targets are detected according to the current data-association hypothesis.

Then, the second term of the equation (3-11) can be written as follow:

$$\begin{aligned}
P(\psi_h | \Omega_g^{k-1}) &= P(N, C, A | \Omega_g^{k-1}) \\
&= P(A | N, C, \Omega_g^{k-1}) P(N, C | \Omega_g^{k-1}) \\
&= P(A | N, C, \Omega_g^{k-1}) P(C | N, \Omega_g^{k-1}) P(N | \Omega_g^{k-1})
\end{aligned} \tag{3-13}$$

where N is the *Number*, C is the *Configuration* and A is the *Assignment*.

Assignment is the conditionally independent of *Number* and Ω_g^{k-1} , if the *Configuration* is given. Therefore this probability can be written as:

$$\begin{aligned}
P(A, N, C | \Omega_g^{k-1}) &= P(A | C) P(N, \Omega_g^{k-1} | C) \\
P(A | N, C, \Omega_g^{k-1}) P(N, \Omega_g^{k-1} | C) &= P(A | C) P(N, \Omega_g^{k-1} | C) \\
&\Downarrow \\
P(A | N, C, \Omega_g^{k-1}) &= P(A | C)
\end{aligned} \tag{3-14}$$

Configuration is conditionally independent of Ω_g^{k-1} , if the *Number* is given.

Therefore, the second term on the right hand side of the equation (3-13) can be expressed with the following equation:

$$\begin{aligned}
P(C, \Omega_g^{k-1} | N) &= P(C | N) P(\Omega_g^{k-1} | N) \\
P(C | N, \Omega_g^{k-1}) P(\Omega_g^{k-1} | N) &= P(C | N) P(\Omega_g^{k-1} | N) \\
&\Downarrow \\
P(C | N, \Omega_g^{k-1}) &= P(C | N)
\end{aligned} \tag{3-15}$$

Then, equation (3-13) can be rewritten as follows:

$$P(\psi_h | \Omega_g^{k-1}) = P(A | C) P(C | N) P(N | \Omega_g^{k-1}) \tag{3-16}$$

Reid [1] assumed that; $N_{DT}(h)$ is given by a binomial distribution, $N_{FT}(h)$ and $N_{NT}(h)$ follow a Poisson distribution. Because of this assumption; the probability of the *Number* Ω_g^{k-1} is calculated with the following equation:

$$\begin{aligned} P(N | \Omega_g^{k-1}) &= P(N_{DT}, N_{FT}, N_{NT} | \Omega_g^{k-1}) \\ &= \binom{N_{TGT}}{N_{DT}} P_D^{N_{DT}} (1 - P_D)^{N_{TGT} - N_{DT}} F_{N_{FT}}(\beta_{FT}V) F_{N_{NT}}(\beta_{NT}V) \end{aligned} \quad (3-17)$$

where P_D is a probability of detection, β_{FT} is a density of false target, β_{NT} is the density of previously unknown (new) target that has been detected and $F_N(\lambda)$ is the Poisson probability distribution for N events when the average rate of events is λ .

The total number of measurements is given by:

$$M_K = N_{DT} + N_{FT} + N_{NT} \quad (3-18)$$

The probability of a specific *Configuration*, given *Number* is given by [1]:

$$P(C | N) = \frac{1}{\binom{M_K}{N_{DT}} \binom{M_K - N_{DT}}{N_{FT}}} \quad (3-19)$$

There are many ways to assign the N_{DT} measurements to the N_{TGT} targets.

The probability of an *Assignment* for a given *Configuration* is given below:

$$P(A | C) = \frac{(N_{TGT} - N_{DT})!}{N_{TGT}!} \quad (3-20)$$

Substituting these three equations in equation (3-17), the probability of the second term of the equation (3-11) can be obtained as:

$$P(\psi_h | \Omega_g^{k-1}) = \frac{N_{FT}! N_{NT}!}{M_k!} P_D^{N_{DT}} (1 - P_D)^{N_{TGT} - N_{DT}} F_{N_{FT}}(\beta_{FT} V) F_{N_{NT}}(\beta_{NT} V) \quad (3-21)$$

Combining and simplifying equations (3-12) and (3-21) give us the final probability, which is

$$P_i^k = \frac{1}{c} P_D^{N_{DT}} (1 - P_D)^{N_{TGT} - N_{DT}} \beta_{FT}^{N_{FT}} \beta_{NT}^{N_{NT}} \left[\prod_{m=1}^{N_{DT}} N(Z_m - H\bar{x}, B) \right] P_g^{k-1} \quad (3-22)$$

3.1.6 Combining

Another hypothesis limitation method is to combine similar tracks with similar effects. Hypotheses that have same number of similar tracks are the candidates for combination.

The similarity of track pairs of hypotheses is measured with respect to two different techniques. The first one is the N-scan criterion in which the last N data scans of tracks in common are combined. For instance, if N is chosen to be two, all tracks with the same observations from the last two scans would be considered similar [9].

Another similarity technique, which is recommended by Reid [1] and used in this thesis, is that both means and the covariances of each track estimate must be sufficiently similar. Track X of the first hypothesis and track Y of the second hypothesis are declared similar if the following criteria are satisfied [9]:

$$|\mu_{X_i} - \mu_{Y_i}| \leq \beta \sqrt{P_{X_{ii}} - P_{Y_{ii}}} \quad (3-23)$$

and

$$P_{x_{ii}} < \alpha P_{y_{ii}}, \quad P_{y_{ii}} < \alpha P_{x_{ii}} \quad (3-24)$$

where μ, P are the means and covariance of each track, i is the index over all the estimation states. Typical α and β values, 2 and 0.1, respectively given in [9] are used in this study.

After the similarity test is completed, hypotheses with lower probabilities are deleted and probabilities of remaining hypotheses become the sum of the probabilities of similar hypotheses.

3.1.7 Pruning

MHT algorithm could require very large amounts of memory if precautions like ‘pruning’ are not used. One technique is to remove hypotheses that have probabilities less than a fixed threshold. Another technique allows only a predetermined fixed number of hypotheses. In this technique, hypotheses are ranked by the probabilities and the M most likely ones are chosen. Another pruning technique is to rank and to sum probabilities of the more likely hypotheses until the sum reaches a threshold. Then remaining hypotheses are deleted. The last one is the N-Scan pruning technique. It first identifies the most likely hypotheses and then pruning is achieved by tracing back N scans from each track in the most likely hypothesis and that node becomes the new root. Branches that do not have the same new root will be deleted.

Considering all these techniques, “remove low probability” hypothesis is used because of the small computational time requirement.

3.1.8 Prediction and Filtering

In this thesis, prediction is performed by a Kalman filter due to its simplicity. In addition, if the system can be assumed to be linear and the measurement noise is to be zero mean white Gaussian, Kalman filter successfully minimizes the variances of the prediction error.

One cycle of the state estimation procedure in the Kalman filter is shown in Figure 3-5, according to the given dynamic equation and measurement equation.

The dynamic (plant) equation is given as:

$$\begin{aligned}x_{k+1} &= Fx_k + \Gamma w_k \\ E[\Gamma w_k w_k^T \Gamma^T] &= Q\end{aligned}\tag{3-25}$$

where x_k is the state vector, Γ is the noise gain and w_k is the zero mean white Gaussian process noise with covariance Q .

The measurement equation is as follows:

$$\begin{aligned}z_k &= Hx_k + v_k \\ E[v_k v_k^T] &= R_k\end{aligned}\tag{3-26}$$

where v_k is the zero mean white Gaussian measurement noise with covariance R_k .

Discrete white noise acceleration (DWNA) model is chosen as a kinematic state model since it is commonly used and has an advantage that the process noise intensity is easily related to physical characteristics of the motion [25].

The transition matrix (F) and the covariance (Q) of DWNA model is given in (3-27) as follows:

$$F = \begin{bmatrix} 1 & T \\ 0 & 1 \end{bmatrix}$$

$$Q = \begin{bmatrix} \frac{1}{4}T^4 & \frac{1}{2}T^3 \\ \frac{1}{2}T^3 & T^2 \end{bmatrix} \sigma_v^2 \quad (3-27)$$

where σ_v^2 is the standard deviation of the process noise.

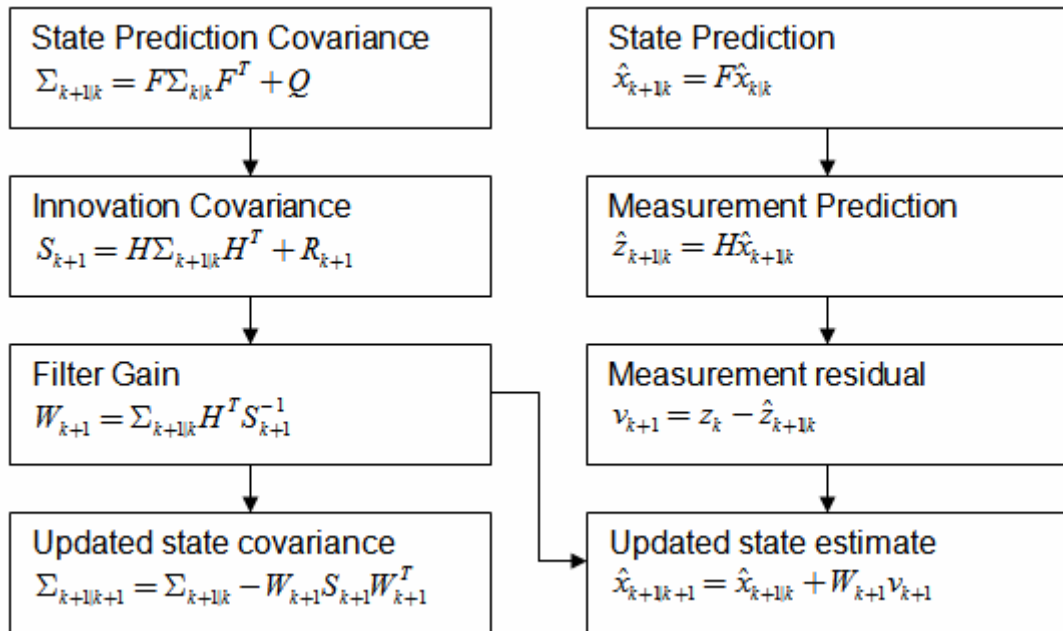


Figure 3-5 One cycle in the state estimation procedure of Kalman filter.

CHAPTER 4

ELECTRONIC ATTACK (EA) TECHNIQUES

EA is a set of actions taken to prevent or reduce the enemy's effective use of the electromagnetic spectrum [10]. Besides EA, Electronic Support (ES) and Electronic Protection (EP) are the other two components of electronic warfare. In radar applications, the main objective is to reject or to falsify information (detection, measurement, discrimination, and classification data) that the radar tries to obtain [10].

EA techniques can be classified in a number of ways. From the point of view whether electromagnetic energy is radiated or not, EA is divided into active and passive. EA can also be divided into angle-measurement EA, range-measurement EA and velocity-measurement EA by considering influenced parameters of radar information. From the point of the types of jammed radars, it can be divided into EA against search (surveillance) radars and EA against tracking radars. From the viewpoint of the EA systems' location, two types of EA are distinguished as onboard or offboard.

In this chapter, the fundamentals of EA are described using the following classification:

- Active EA
- Passive EA

Next RGPO model which is selected to be modeled as an EA technique in this work is explained in detailed.

4.1 EA TYPES

4.1.1 Active EA

Active EA incorporates devices and methods based on deliberate radiation of electromagnetic energy to disrupt the operation of the victim radar [10]. Corresponding techniques are described under two fundamental types: noise jamming and deception jamming. Since there are several techniques of noise and deception jamming, for the sake of the simplicity only more common types of them are discussed in this section.

4.1.1.1 Noise Jamming

This is the case where a jammer transmitting a noise-like signal for the purpose of increasing the radar receiver noise level. An optimum jamming signal has the characteristics of receiver noise develops on its own, so the operator may think that his own receiver noise figure has increased. However the operator will be easily able to discriminate the presence of noise jamming in the presence of very high power noise. The major

advantage of this type of jamming is that only little information about the victim radar equipment is necessary.

This type of jamming is known to be more effective against search radars than against tracking radars [10]. The most common types of noise jamming are explained in the following subsections.

4.1.1.1.1 Spot Noise Jamming

Spot noise jamming radiates narrowband noise like energy to mask either the range or the presence of targets. Its bandwidth is just wide enough to cover the victim radar bandwidth and power is concentrated at the victim radar's signal frequency. It can be used for self-screening, for mutual support missions and for standoff missions. Only fixed-frequency radar is expected to be affected by the spot noise jamming, efficiently.

4.1.1.1.2 Barrage Noise Jamming

When the victim radar is frequency agile or uses techniques of the spread spectrum, noise jamming must cover a wider band and this type of noise jamming is called barrage noise jamming. Its bandwidth is designed to cover the radar's whole agile bandwidth simultaneously and this feature distinguishes the barrage noise jamming from the spot noise jamming.

4.1.1.1.3 Frequency-Swept Jamming

Frequency-swept jamming is used when the victim radar's instantaneous bandwidth cannot be covered by the noise jammer bandwidth, or when

more than one frequency is used by one or more victim radars. The jammer may then be forced to sweep the jamming energy in a spot bandwidth over the possible range of radar operational frequencies. It can be used against both tracking and search radars to hide the range of the platform being protected.

4.1.1.2 Deception Jamming

Deception jamming is the deliberate transmission or retransmission of amplitude, frequency, phase or otherwise modulated intermittent or continuous wave (CW) signals for the purpose of misleading in the interpretation or use of information by a radar system [16].

This type of jamming is more efficient than noise jamming since it uses a jamming waveform for which the radar receiver is matched. Moreover, less energy is required to jam radar than an equivalent noise jamming.

The main deception jamming techniques against range tracking system, Range Gate Pull-Off (RGPO), against velocity tracking system, Velocity Gate Pull-Off (VGPO), and against angle tracking system, cross polarization, cross eye, blinking and inverse gain, are described following subsections.

4.1.1.2.1 Range Gate Pull-Off (RGPO)

RGPO is a range-measurement EA technique in which a repeater captures the tracking range gate and moves the gate away from the target echo, then turns off to leave the range gate with no signal (Figure 4-1). At the

beginning, the repeater pulse amplified smoothly to a level sufficient to suppress the target echo pulse. Then, the repeater pulse is delayed (possible for PRF stagger or carrier frequency agile radars) or advanced to pull the gate off the target echo. When the target echo is not contributing to the output of the gate, the repeater pulse is turned off and only the thermal noise of the receiver will then remain in the range gate, which implies breaking the tracking loops.

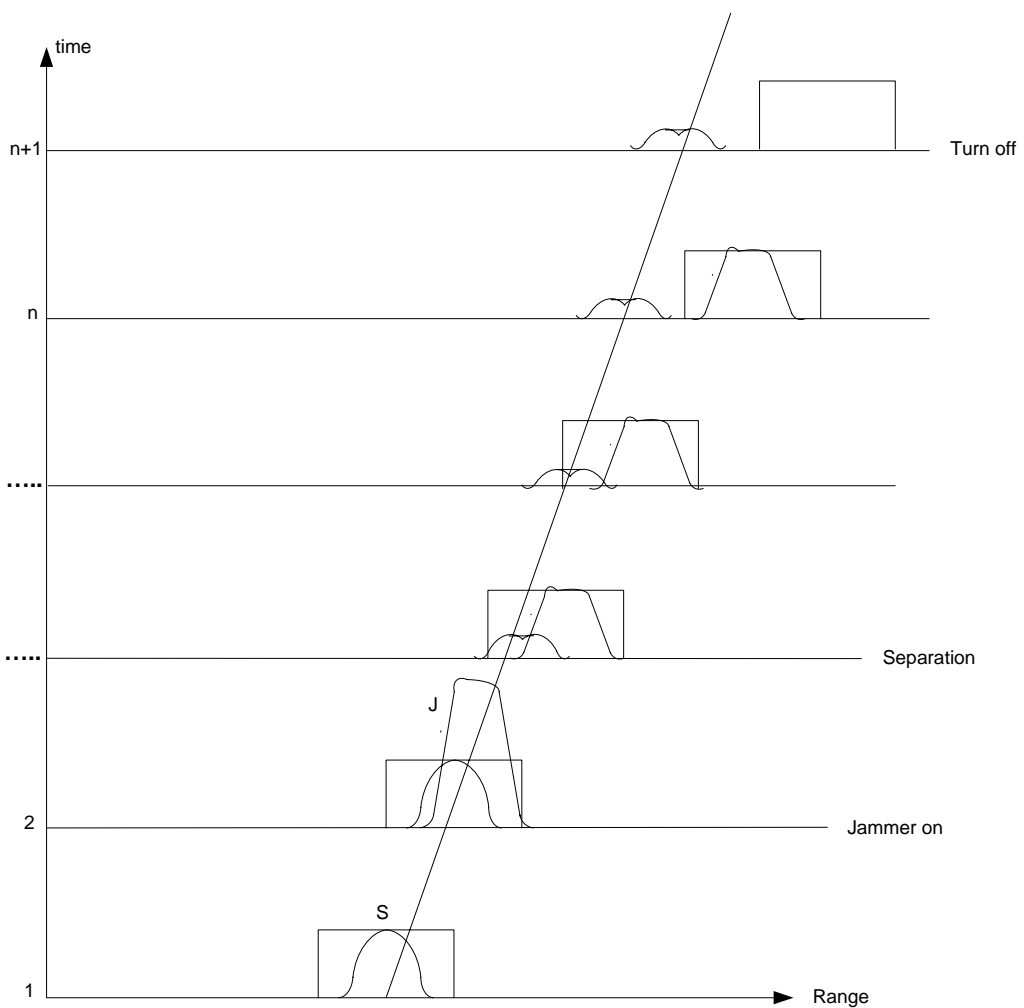


Figure 4-1 Range gate pull-off (RGPO).

Range gate pull-off (RGPO) has the potential to be very effective against tracking radar [15]. It is also known as the range gate walk-off, range-gate capture and range gate stealing.

4.1.1.2.2 Velocity Gate Pull-Off (VGPO)

Velocity Gate Pull-Off (VGPO) is particularly important against tracking radars (pulsed or CW) which employ Doppler filters (called speed gates) in their angle-tracking loops [22].

The jammer reradiates the target signal at a high jammer- to-signal ratio to capture the radar velocity-tracking gate. Next, it pulls the captured gate off the true target Doppler signal and for a moment switching off the jammer signal to cause break-lock. When the flying missile is considered, reacquisition of the target could be extremely difficult. This technique is also known as velocity or Doppler gate capture, walk-off or stealer.

4.1.1.2.3 Cross Polarization Jamming

This EA technique exploits the fact that radiating the signal whose polarization is orthogonal to the victim radar receiving antenna causes angular errors in tracking radars. This situation is depicted in Figure 4-2, where normal polarized and cross-polarized signal responses are opposite to each other.

Measuring the polarization of the victim radar and retransmitting a signal with a correct orthogonal polarization are two requirements of utilizing cross polarization jamming.

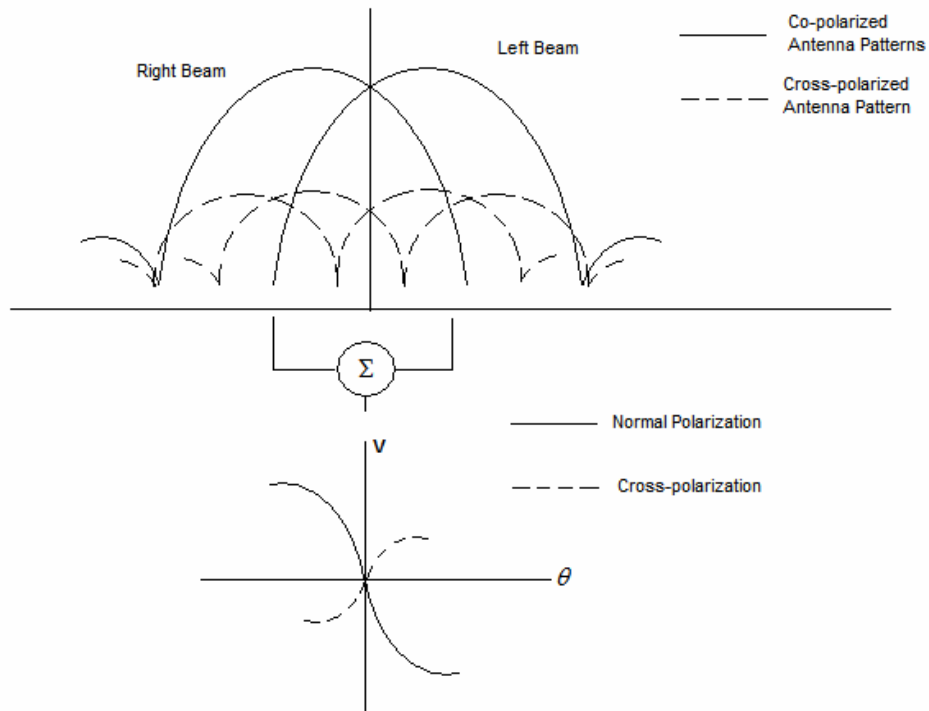


Figure 4-2 Cross polarization jamming of monopulse radar [22].

4.1.1.2.4 Cross Eye Jamming

A cross-eye system depends on the fact that phase distortion of the wavefront causes an angular error in the victim radar. This distortion is obtained when the two coherent sources separated by a distance L , generates jamming signals that arrive at the victim radar matched in amplitude but 180 degrees out of phase. The cross-eye technique is often regarded as difficult to implement since it requires very advanced technologies [15].

4.1.1.2.5 Blinking Jamming

Blinking jamming is a noncoherent multiple-source jamming executed by with several jamming transmitters that alternatively turns on and off, at about a %50 duty cycle. It is an effective electronic attack against guided missiles using radar seekers, when the jamming transmitters located on different platforms are used, the main aim of this jamming is to make a missile wander from one platform to another, as a result, it wanders between the platforms without hitting them. The accurate choice of the exchange rate increases the effectiveness of this jamming. Too low rate permits the radar to decide the real position of each target and too high rate causes tracking radar minimize the angular error by averaging the data.

4.1.1.2.6 Inverse Gain Jamming

Inverse gain jamming provides a deception or noise jamming with amplitude modulation which is the inverse of the victim radar combined transmit and receive antenna scan patterns. It is used for against scanning-type search radar, tracking radar in acquisition mode, active conical scan tracking radar and active track-while-scan radars [16].

4.1.2 Passive EA

Passive EA involves devices reflecting electromagnetic energy to hide real reflection. Typical types of passive EA are chaff and passive decoy.

4.1.2.1 Chaff

Chaff is made up of clouds of metal strips or metallic materials that can be floated or suspended in the atmosphere to create a high radar return zone for concealing the presence of true targets or to confuse victim electronic system (Figure 4-3). It is used for airborne operations to hide the approach of attacking aircraft by creating chaff corridors or for ships as a countermeasure against RF-guided missile or search radars.

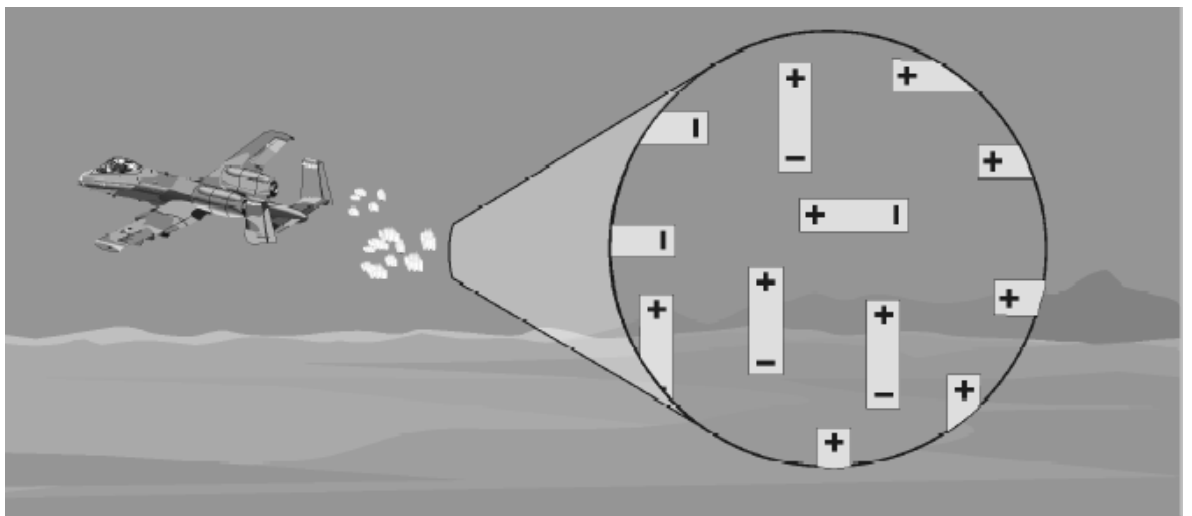


Figure 4-3 Polarizations of chaff [23].

4.1.2.2 Passive Decoy

The basic concept underlying the passive decoy technique is a simple expendable device capable of reproducing a radar signature at least as attractive to enemy weapon systems as the signature of the platform to be protected [15]. Luneberg lens reflectors, corner reflectors, balloons covered with conductive coverings and large metallic screens can be used as a passive decoy to reflect radar energy (Figure 4-4).

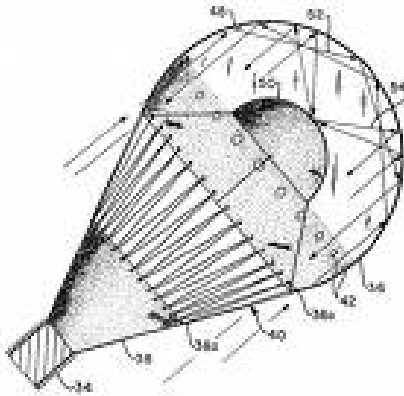


Figure 4-4 Passive decoy.

4.2 EA MODEL

After examining the most common types of EA techniques, RGPO technique against track radar was selected to be modeled due to the reasons given below. Noise jamming type techniques were eliminated because; they are more effective electronic attack against search radars than tracking radars. Cross-eye and cross-polarization jamming are difficult to implement since they require very advanced technologies so they are not in widespread usage. Blinking jamming was eliminated because it is an effective electronic attack against guided missiles using radar seekers. VGPO is a deception technique against tracking radars, which use Doppler filters, but our tracking radar does not include Doppler processing. Also inverse gain jamming is not proper since it is used against radars that utilize beam-scanning techniques. It is very complicated to model chaff and passive decoy with all the parameters which have influence on their success.

Besides all these reasons, RGPO is a fundamental deception EA technique employed against automatic tracking radars [22].

4.2.1 RGPO Model

In RGPO, the repeater pulse is amplified and delayed to pull the gate off the target echo. Linear and parabolic are the two modes of time delay controller of RGPO (Figure 4-5).

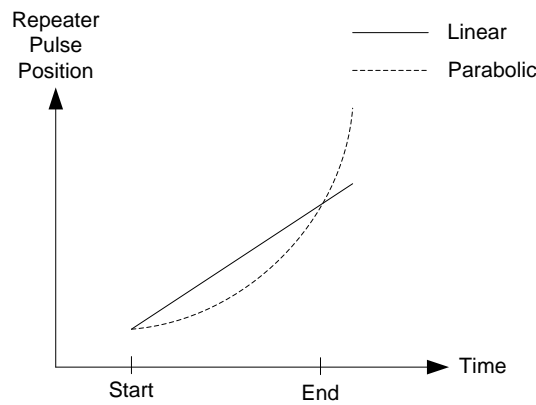


Figure 4-5 Repeater pulse position for two modes.

For the linear case, the range of the false target with respect to the radar is written as [13]:

$$R_{FT} = R_T + V(t_k - t_0) \quad (4-1)$$

where R_T is the range of the actual target, V is the rate of pull-off, t_k is the time of radar dwell and t_0 is the initial reference time of the RGPO false target.

For the parabolic case, the range of the false target with respect to the radar is expressed as [13]:

$$R_{FT} = R_T + \frac{1}{2}A(t_k - t_0)^2 \quad (4-2)$$

where A is the acceleration of pull-off of the false target.

The measurement of the RGPO will be generated by modification of equation (2-13) as follows:

$$P_r^{FT}(t) = \frac{P_t G^2 \lambda^2 \sigma(t) \gamma}{(4\pi)^3 R_{FT}(t)^4 L_{total}(t)} F_{sum}^2(\theta_T^{az}, \theta_T^{el}) \quad (4-3)$$

where γ is the amplification factor of the RGPO.

CHAPTER 5

OPTIMIZATION

The main purpose of this thesis is to find optimized parameters of tracking radar simulator. Moreover, RGPO parameters are optimized against tracking radar simulator with optimum parameters for developing the model. These optimization problems have multiple local optimum points. Genetic Algorithm (GA) is a suitable optimization technique that can be applied to these kinds of problems. Here, in this thesis, MATLAB GA tool is used. The block diagram of simulation environment is given in the following figure.

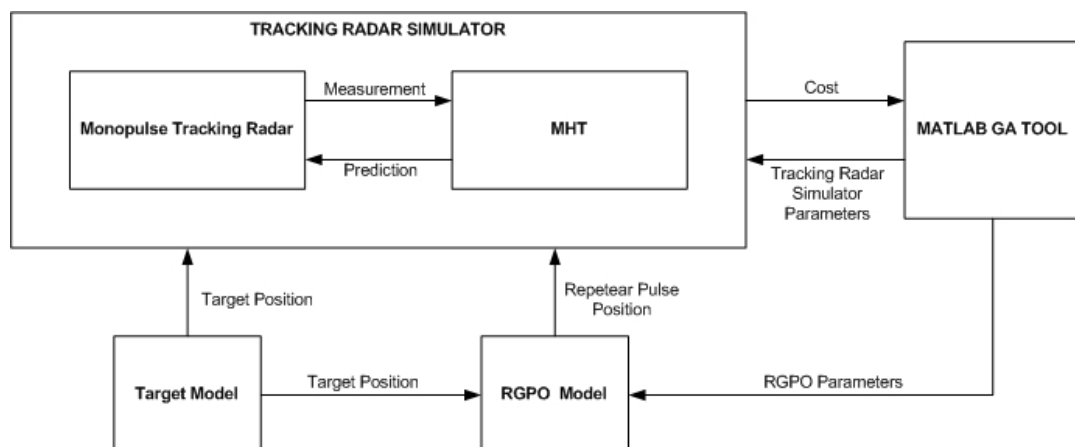


Figure 5-1 Block diagram of simulation environment.

In this chapter, parameters of the tracking radar simulator and the parameters, which are supposed to be the optimization problem variables, are introduced first. After describing the cost function construction, scenarios for optimization of tracking radar simulator and RGPO are given. Finally, a brief explanation of GA is given as a tool for solving the optimization problem.

5.1 PARAMETERS AND CONSTRAINTS

Three groups of parameters of simulation environment are tracking radar parameters, tracker (MHT) parameters and RGPO parameters. Tracking radar parameters are also divided into two subgroups: antenna parameters and receiver parameters. These parameters are listed in Table 5-1, Table 5-2 and Table 5-3, respectively. Furthermore; default values, parameter ranges and types of these parameters are given in these tables. Parameter type shows that if it is a variable of the optimization problem or not (fixed).

Table 5-1 Parameters of tracking radar.

<i>Antenna Parameters</i>	<i>Default Value</i>	<i>Range</i>	<i>Type</i>
Beamwidth Az/El (deg)	2	0-90	Fixed
Max. Side lobe Level Az/El (dB)	0.4	0-1	Fixed
Aperture Efficiency	0.8	-	Fixed
Number of Array Elements on z and x plane	200	-	Fixed
Displacement between two neighbor array element on z and x plane	0.015	-	Fixed
<i>Receiver Parameters</i>	<i>Default Value</i>	<i>Range</i>	<i>Type</i>
Transmitter peak power (Watt)	500000	-	Fixed
Pulse width (m)	7.5	-	Fixed
Band width (MHz)	20	-	Fixed
Carrier frequency (GHz)	2	-	Fixed
Dispative loss (dB)	1	-	Fixed
Transmission line loss (dB)	1	-	Fixed
Noise figure (dB)	2	-	Fixed
IF gain (dB)	1	-	Fixed
Probability of false alarm	1e-7	0-1	Fixed
Detection threshold (Watt)	1.29e-6	-	Fixed
Range gate width (m)	3000	15-150	Variable

Table 5-2 Parameters of MHT.

<i>Parameters</i>	<i>Default Value</i>	<i>Range</i>	<i>Type</i>
Update interval of radar (sec)	0.05	-	Fixed
Maximum expected velocity of target (m/sec)	400	-	Fixed
Probability of detection	0.9	0.5-1	Variable
Density of false target	0.1	-	Fixed
Density of new target	0.5	-	Fixed
Gate threshold gamma	25	-	Fixed
Range measurement noise variance (m ²)	7.5	-	Fixed
Azimuth measurement noise variance (deg ²)	2.3e-5	-	Fixed
Elevation measurement noise variance (deg ²)	2.3e-5	-	Fixed
Process noise standard deviation of CV model (m/sec ²)	25	1-50	Variable
Threshold for pruning	0.2	0.1-0.5	Variable
Constant of similarity criteria for combining hypothesis, beta	0.1	-	Fixed
Constant of similarity criteria for combining hypothesis, gamma	2	-	Fixed
Confirmed target threshold	0.99	0.7-1	Variable

Table 5-3 Parameters of RGPO.

<i>Parameters</i>	<i>Default Value</i>	<i>Range</i>	<i>Type</i>
Rate of pull-off for linear case (m/sec)	30	0-500	Variable
Acceleration for pull-off for parabolic case (m/sec ²)	2	0-80	Variable
Initial reference time (sec)	20	10-50	Variable
End time (sec)	40	10-80	Variable
Amplification factor	2	1-4	Variable

All of the track radar parameters except the range gate width are set to a fixed value. Default values of them are chosen from the results of [4]. Range gate width is selected to be an optimization parameter besides tracker parameters because we notice in our tests that tracking performance is highly dependent on its value especially in the crossing targets case. Also, the EA technique to be developed is affected by its value.

Among the MHT parameters, maximum expected velocity of target is selected to be fixed because it just shows maximum speed of target that radar can be tracked. Also range, azimuth and elevation measurements' noise variances are assumed to be fixed parameters because they depend on receiver and antenna design. Constants of similarity criteria alpha and gamma are taken the fixed values given in [9]. Other parameters are the variable parameters of optimization problem.

All of the RGPO parameters are among the optimization problem variables because all of them describe the deception techniques and none of them can take system specific values.

5.2 COST FUNCTION

In our optimization problem, variables and their ranges are introduced in the previous section. Now, the cost function of the optimization problem should be constructed. Cost function of our problem is composed of three parts as shown below:

$$Cost = \sum_{l=1}^L w_l (TrackErrorCost_l + FalseTrackCost_l + TrackLossCost_l) \quad (5-1)$$

where L is the number of scenarios and w_l is the weight of the l^{th} scenario.

First cost element represents the total tracking error and its job is to minimize the tracking error. It is calculated as

$$TrackErrorCost = \sum_{k=1}^M \left[\sum_{j=1}^N \left[\sqrt{\sum_{i=1}^3 (z_i - \hat{z}_i)^2} \right] \right] \quad (5-2)$$

where M is the number of dwells, N is the number of targets, z_i is the true target position of the i^{th} coordinate and \hat{z}_i is the predicted target position of the i^{th} coordinate.

Radar must track only true targets, so false target tracking should always be punished. For this reason, second element is formed as

$$FalseTrackCost = 1000 \sum_{k=1}^M (x_k) \quad (5-3)$$

where x_k is the number of false track at k^{th} dwell.

Track maintenance is another requirement that radar must satisfy. Last element expresses of this requirement as

$$TrackLossCost = 10^6(n_{Target} - n_{Track}) \quad (5-4)$$

where n_{Target} is total number of targets and n_{Track} is the total number of tracks in the scenario.

5.3 OPTIMIZATION SCENARIOS

5.3.1 Multi-Target

Seven different multi-target scenarios are prepared to be used in the optimization of tracking radar simulator parameters. Six scenarios are involved with two targets whose models are developed by us. First three scenarios represent special target motions and all target velocities are taken constant. Target motions in other three scenarios are accelerated versions of the first ones. Target models of the last scenario which are used for benchmark problem in [13] are taken to evaluate the tracker performance under real target models.

5.3.1.1 Scenario 1

This scenario consists of two targets flying in parallel with constant velocities. The motion characteristics are given at Table 5-4. The trajectory of the target models can be examined from Figure 5-2 and Figure 5-3. The initial target positions in 3D path figure are marked by stars.

Table 5-4 Motion characteristics of target models in scenario 1.

		Initial Position (m)	Final Position (m)	Velocity (m/sec)	Acceleration (m/sec ²)	Total time (sec)
Target 1	X	18000	21595.5	90	0	40
	Y	42000	43598	40	0	
	Z	900	700.25	-5	0	
Target 2	X	17000	21794	120	0	
	Y	45000	46198.5	30	0	
	Z	2000	1800.25	-5	0	

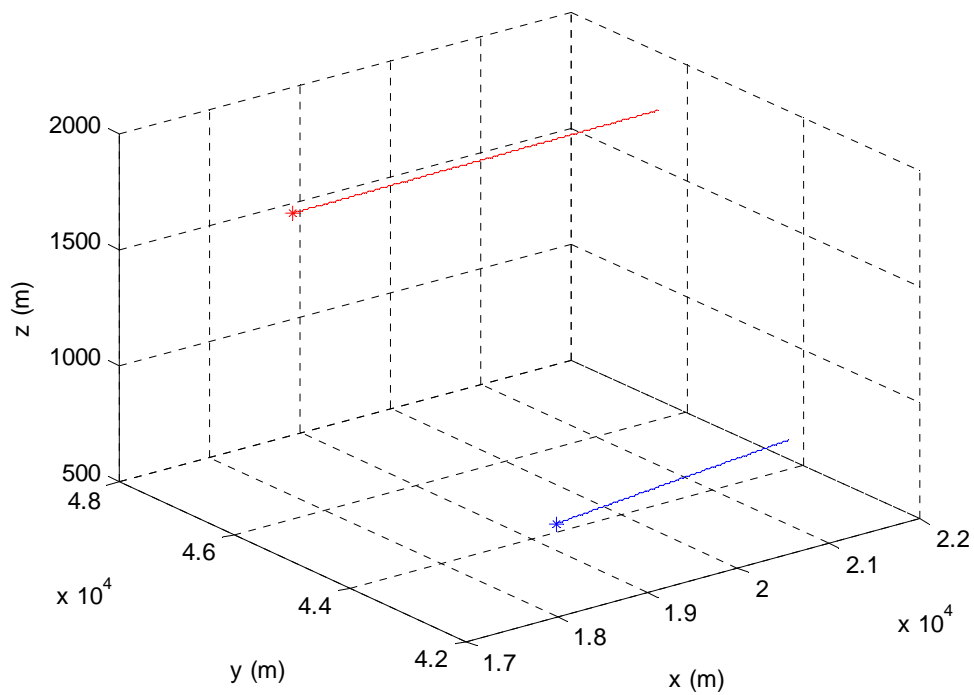


Figure 5-2 The 3D path of target models in scenario 1.

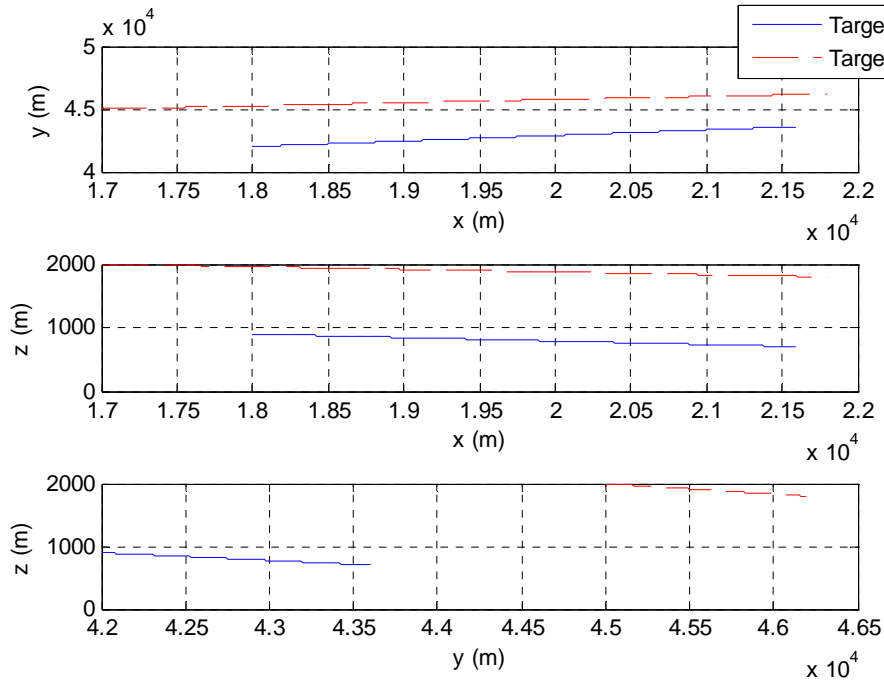


Figure 5-3 Target trajectories on two coordinates in scenario 1.

5.3.1.2 Scenario 2

Two crossing targets in x coordinate are modeled in this scenario. The purpose of this scenario is to evaluate the tracking radar simulator performance for closely spaced targets. The motion characteristics are given at Table 5-5. The target models can be examined from Figure 5-4 and Figure 5-5.

Table 5-5 Motion characteristics of target models in scenario 2.

		Initial Position (m)	Final Position (m)	Velocity (m/sec)	Acceleration (m/sec ²)	Total time (sec)
Target 1	X	15000	9007.5	-150	0	40
	Y	12000	12000	0	0	
	Z	5000	5000	0	0	
Target 2	X	10000	13196	80	0	
	Y	12000	12000	0	0	
	Z	5000	5000	0	0	

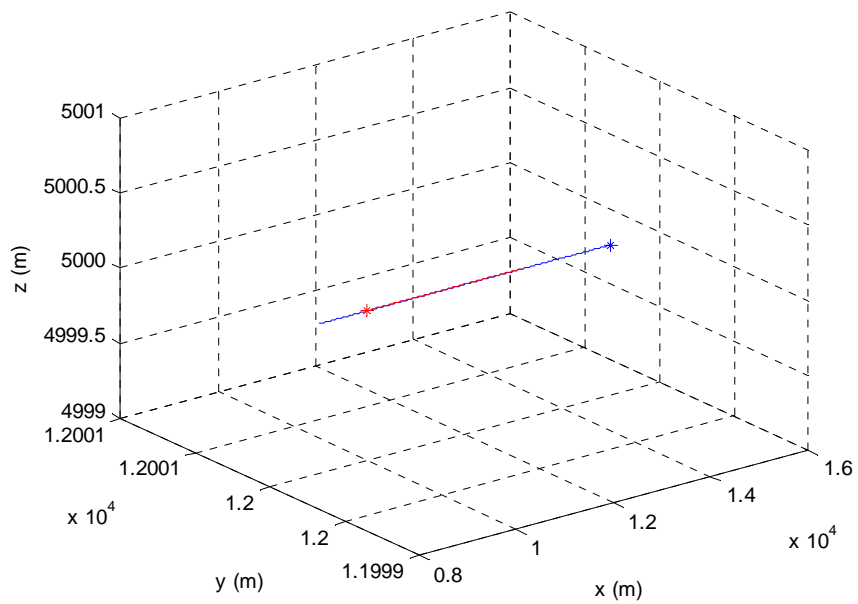


Figure 5-4 The 3D path of target models in scenario 2.

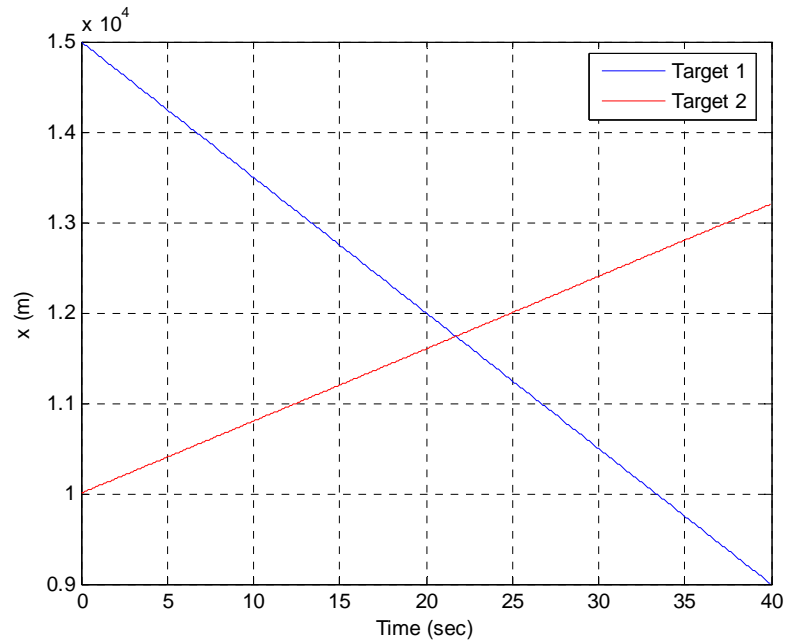


Figure 5-5 Target trajectories on the x coordinate in scenario 2.

5.3.1.3 Scenario 3

In scenario 3, two targets maneuver and separate rather than crossing. Targets become nearer up to the twenty-five seconds. Then they fly away each other. The motion characteristics are given at Table 5-6. Target trajectory in the x-y-z coordinates is given in Figure 5-6 and Figure 5-7. Also, Figure 5-8 shows how close the targets in the y coordinate is.

Table 5-6 Motion characteristics of target models in scenario 3.

		Initial Position (m)	Final Position (m)	Velocity (m/sec) Min/Max	Acceleration (m/sec ²) Min/Max	Total time (sec)
Target 1	X	20000	20000	0/0	0	45
	Y	16000	15340.47	- 210/258.1	0/12.5	
	Z	1050	1050	0/0	0	
Target 2	X	20000	20000	0/0	0	
	Y	10000	11172.56	- 144.6/135	-8/0	
	Z	850	850	0/0	0	

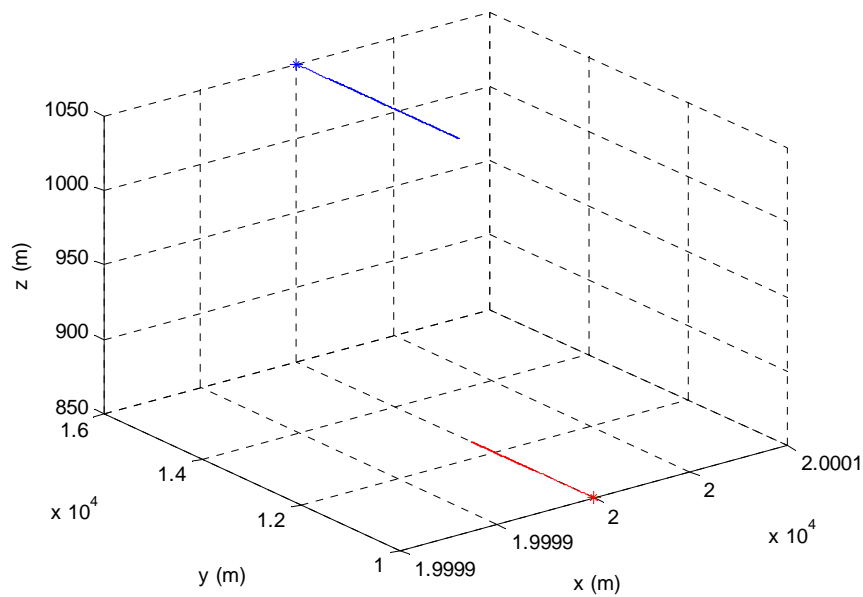


Figure 5-6 The 3D path of target models in scenario 3.

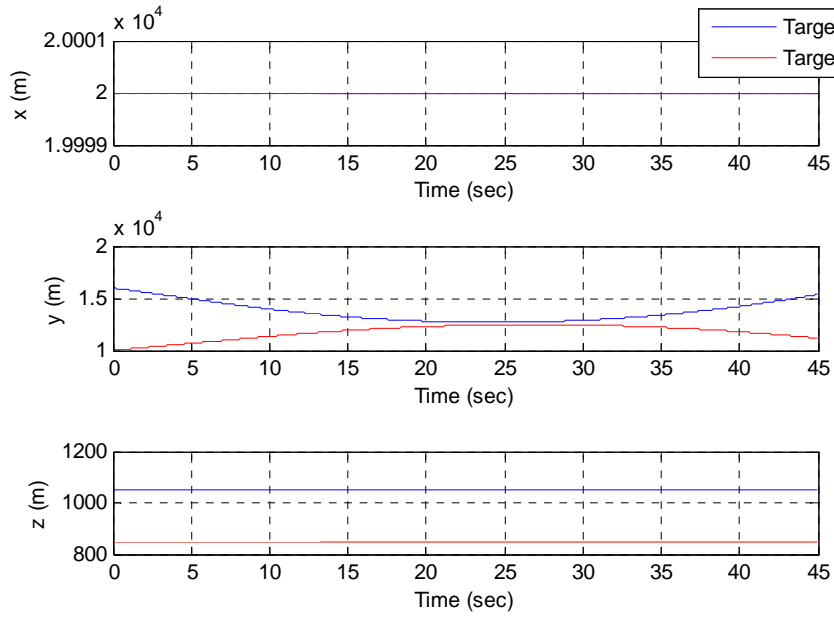


Figure 5-7 Target trajectories on one coordinate in scenario 3.

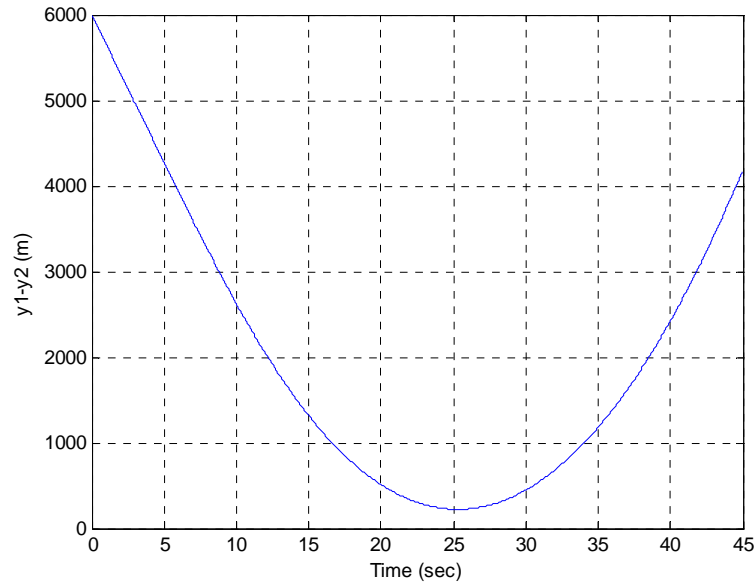


Figure 5-8 Difference of the two target trajectory on the y coordinate.

5.3.1.4 Scenario 4

This scenario is similar to the first one, except that two targets have acceleration on three axes. The motion characteristics are given at Table 5-4. The trajectory of the target models can be examined from Figure 5-9 and Figure 5-10.

Table 5-7 Motion characteristics of target models in scenario 4.

		Initial Position (m)	Final Position (m)	Velocity (m/sec) Min/Max	Acceleration (m/sec ²) Min/Max	Total time (sec)
Target 1	X	18000	21816.7	90/115.5	0/2.55	40
	Y	42000	46866.12	40/215	0/10	
	Z	900	687.8	-7.48/-5	-0.25/0	
Target 2	X	17000	22015.2	120/145.5	0/2.55	
	Y	45000	49466.6	30/205	0/10	
	Z	2000	1787.8	-7.48/-5	-0.25/0	

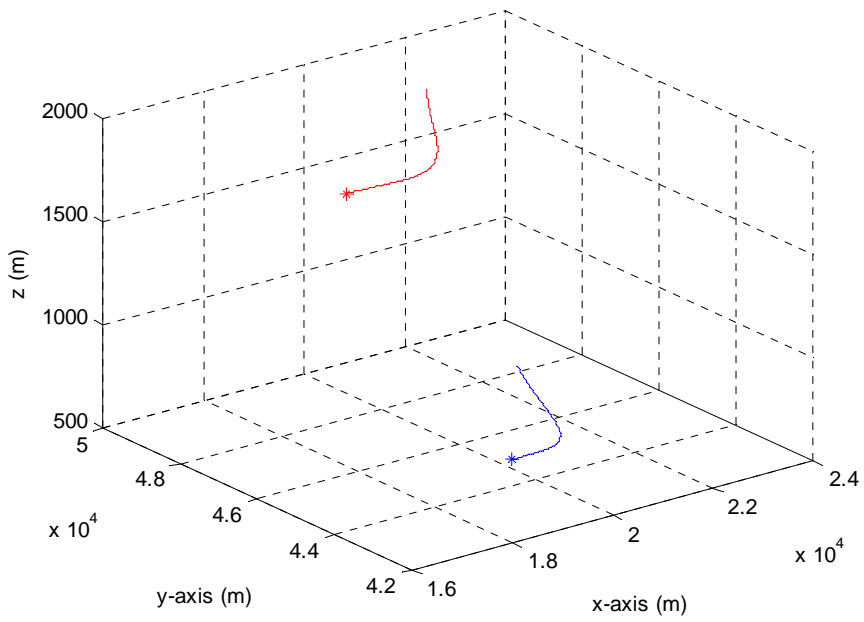


Figure 5-9 The 3D path of target models in scenario 4.

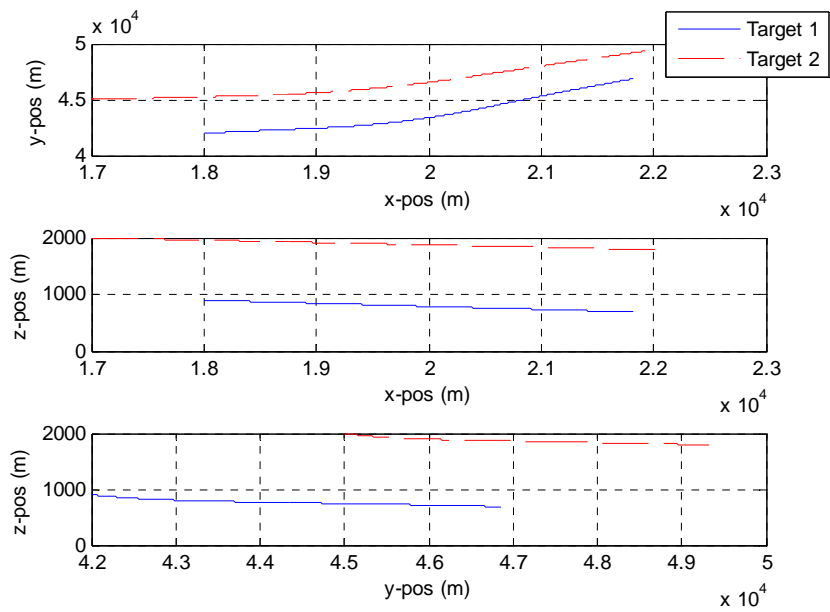


Figure 5-10 Target trajectories on two coordinates in scenario 4.

5.3.1.5 Scenario 5

Accelerated versions of target models in scenario 2 are included in this scenario. The motion characteristics are given at Table 5-5. The target models can be examined from Figure 5-11, Figure 5-12 and Figure 5-13.

Table 5-8 Motion characteristics of target models in scenario 5.

		Initial Position (m)	Final Position (m)	Velocity (m/sec) Min/Max	Acceleration (m/sec ²) Min/Max	Total time (sec)
Target 1	X	15000	8878.83	-170.5/-150	0/-2.55	40
	Y	12000	12060	0/3.73	0/0.25	
	Z	5000	5311.27	0/24.93	0/1.249	
Target 2	X	10000	13285.29	80/94.25	0/2.5	
	Y	12000	11883.65	-5.6/0	-1.25/0	
	Z	5000	4931.41	-5.6/0	-0.5/0	

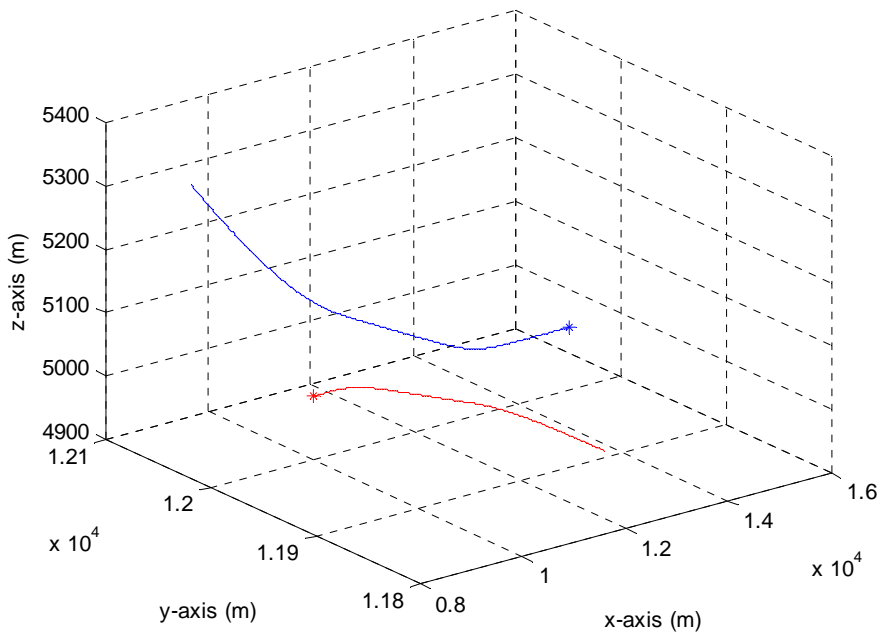


Figure 5-11 The 3D path of target models in scenario 5.

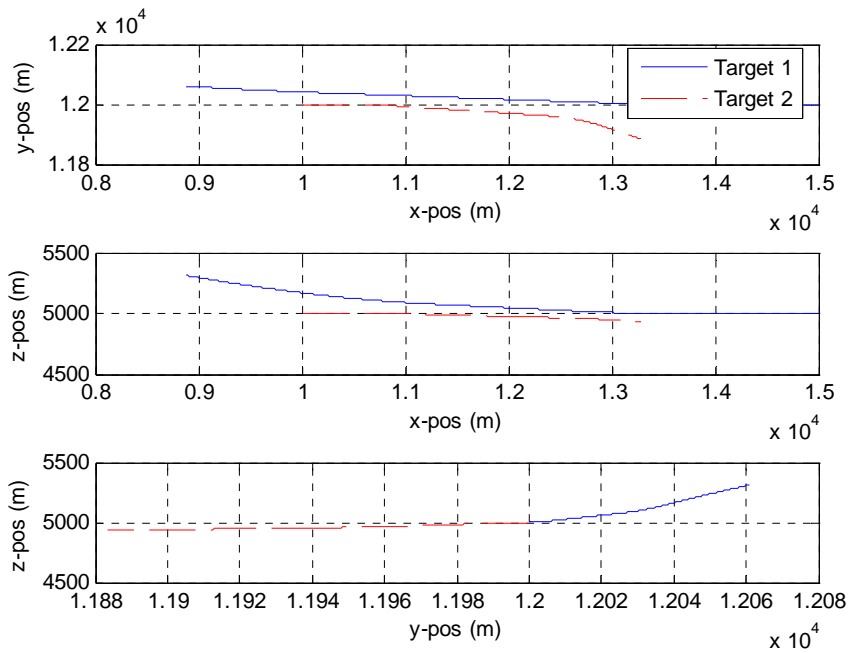


Figure 5-12 Target trajectories on two coordinates in scenario 5.

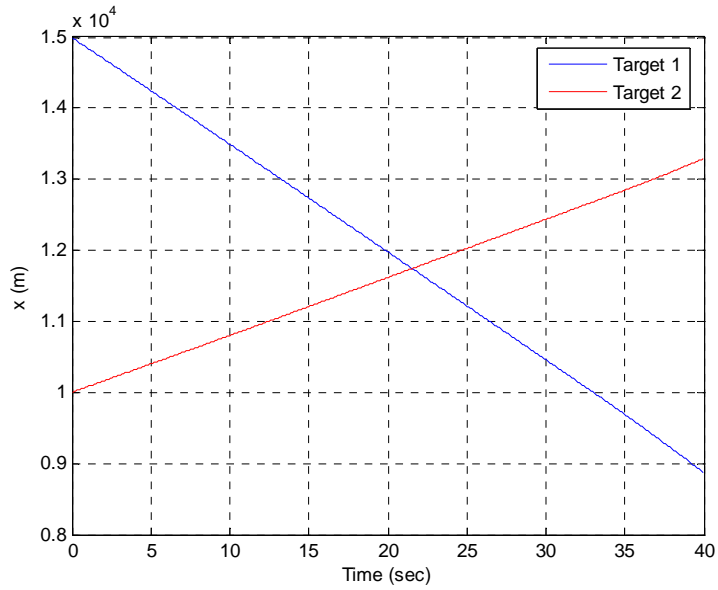


Figure 5-13 Target trajectories on the x coordinate in scenario 5.

5.3.1.6 Scenario 6

It is the same as scenario 3, two targets come closer up to first 20 seconds and then they fly away from each other. Both of the targets have accelerations on three coordinates. The motion characteristics are given at Table 5-9. The trajectory of the target models can be examined from Figure 5-14 and Figure 5-15. Moreover, closeness of targets in the y coordinate is shown in Figure 5-16.

Table 5-9 Motion characteristics of target models in scenario 6.

		Initial Position (m)	Final Position (m)	Velocity (m/sec) Min/Max	Acceleration (m/sec ²) Min/Max	Total time (sec)
Target 1	X	20000	22219.25	0/87.5	-5/5	45
	Y	16000	14955.59	- 210/320.3	0/17.5	
	Z	1050	1260.28	0/9.37	-1.25/1.25	
Target 2	X	20000	18746.08	-103.97/0	-5/0	
	Y	10000	8849.99	- 270.6/135	-12.5/0	
	Z	850	620.58	-8.1/0	-2.47/0.075	

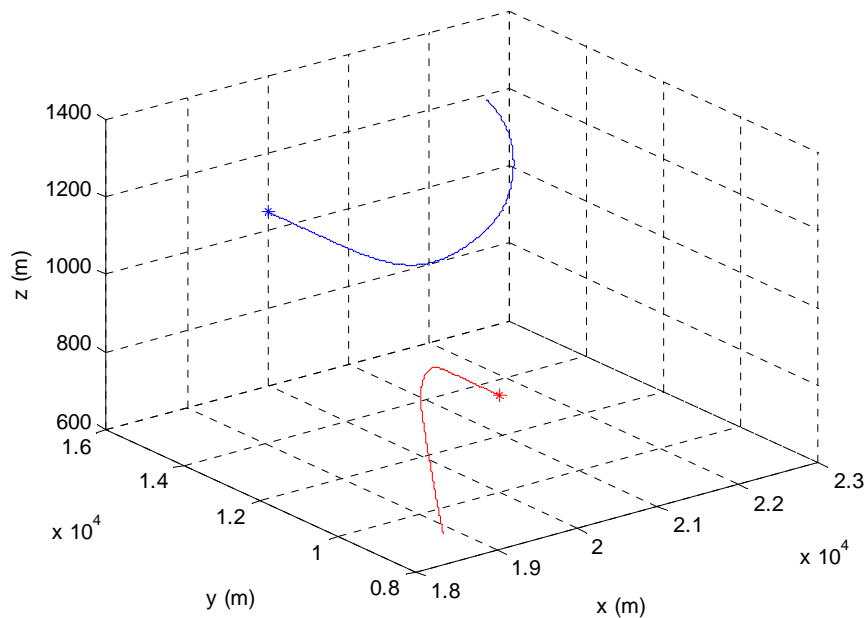


Figure 5-14 The 3D path of target models in scenario 6.

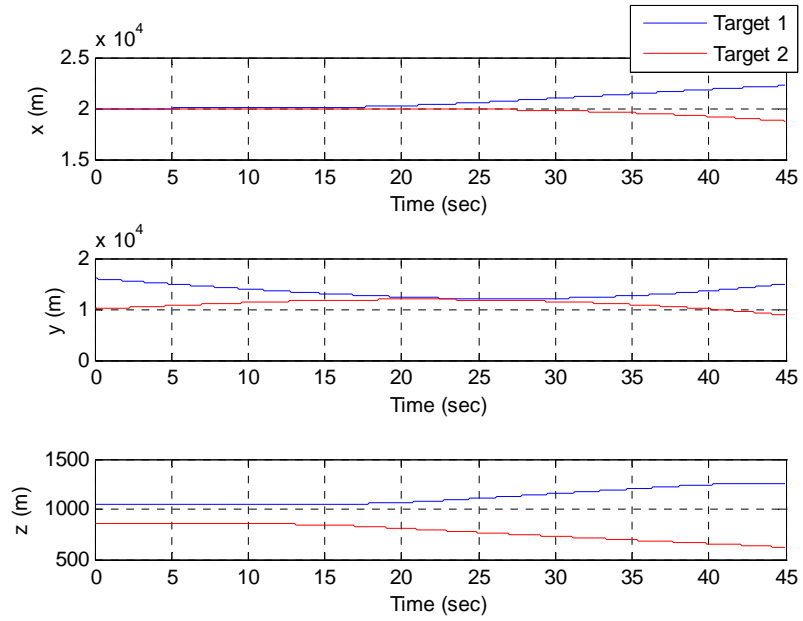


Figure 5-15 Target trajectories on one coordinate in scenario 6.

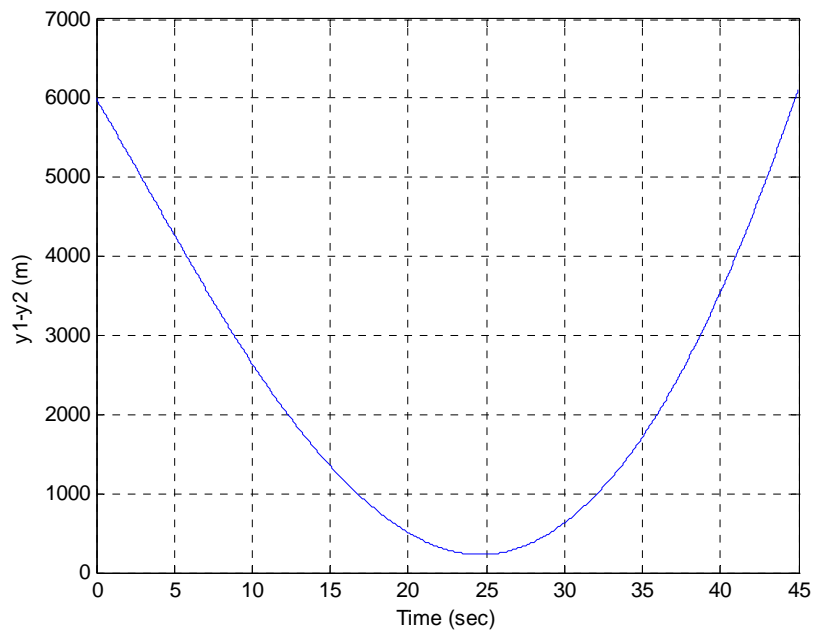


Figure 5-16 Difference of the two target trajectory on the y coordinate.

5.3.1.7 Scenario 7

As mentioned before, six target models in [13] are used in Scenario 7. At the beginning of the scenario, only Target 3, 4 and 5 exist. Target 1 and 2 appear at forty fifth seconds. Target 3 disappears at fifty fifth seconds. Finally, Target 6 comes into sight at sixtieth seconds. The motion characteristics given at Table 5-10 are taken from [4]. Target trajectory is given in Figure 5-17.

Table 5-10 Motion characteristics of target models in scenario 4.

		Initial Position (m)	Final Position (m)	Velocity (m/sec) Min/Max	Acceleration (m/sec ²) Min/Max	Total time (sec)
Target 1	X	61309.3	54573.2	-2.95/-258.89	0/17.06	35
	Y	23646.12	17030.13	-289.59/-129.6	-16.45/0	
	Z	1258	1258	-1.49/3.56	-5.48/6.7	
Target 2	X	32783.37	32289.9	-149.29/14.08	-7.92/22.55	35
	Y	-40737.1	- 30199.25	265.78/304.86	-1.21/10.97	
	Z	4572	3843.8	-32.21/0.03	-12.19/0.6	
Target 3	X	60943.84	49353.21	-323.05/0	-1.2/3.77	55
	Y	60943.84	40374.41	-457.3/-323.05	-2.56/4.87	
	Z	3048	3048	-2.40/5.39	-7.9/7.3	
Target 4	X	30480	21159.82	-268.37/0	-36.57/53	80
	Y	9139.28	-7151.5	-275.05/229.05	-2.43/57.91	
	Z	2286	2286	-2.71/0.94	-8.53/3.65	
Target 5	X	80950.24	58057.3	0/-452.71	-32.3/66.44	80
	Y	969.75	16214.02	0/430.89	-46.9/67.05	
	Z	1448	1448	-0.45/1.4	-1.82/5.48	
Target 6	X	50351.19	49095.1	-287.79/0	-56.08/0	20
	Y	18499.28	10917.38	-426.7/-175.96	-10.3/51.81	
	Z	1548	807.64	-167.97/0	-67.05/48.7	

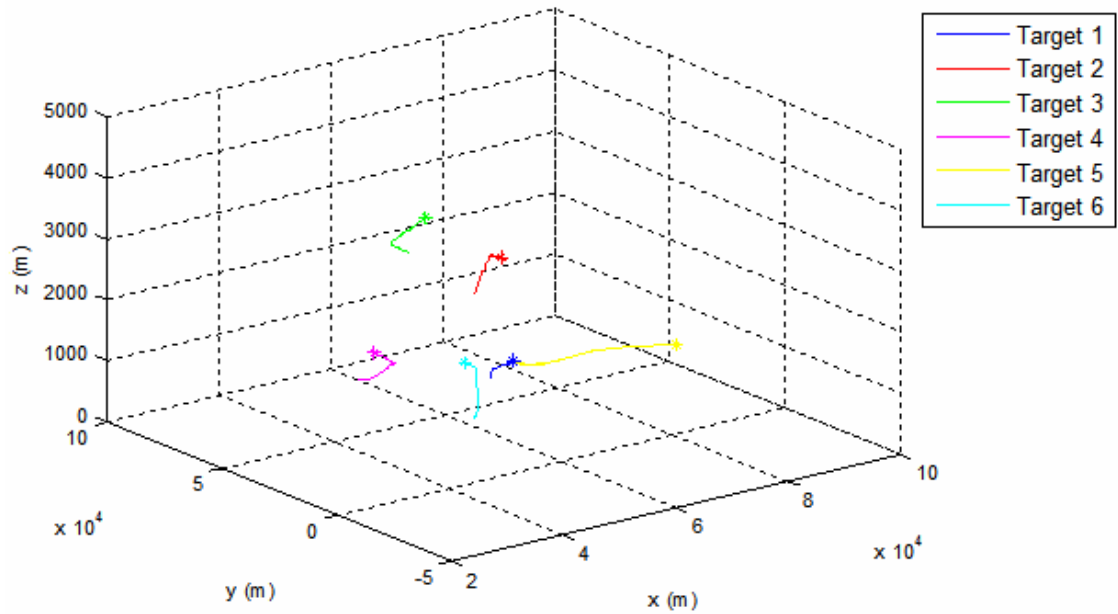


Figure 5-17 The 3D path of target models in scenario 7.

5.3.2 Single-Target

Tracker parameter optimization should be performed in a multi target tracking environment, therefore multi-target scenarios were prepared in last section. When the optimum parameters will be found, RGPO parameters should be optimized by using them in tracker. In that case, we must consider the optimization environment as a target point of view. It does not matter how many targets are there for the target, which uses RGPO as an EA technique. Also, RGPO parameters are not influenced by other targets. Therefore, single target scenarios are used for the optimization of RGPO parameters.

Six target models in [13] are chosen for six single target scenarios. Only first eighty seconds of target motions are employed due to the abbreviation of

optimization duration. The motion characteristics are given at Table 5-11. Further explanations of target models are available in [13].

Table 5-11 Six target models motion characteristics.

		Initial Position (m)	Final Position (m)	Velocity (m/sec) Min/Max	Acceleration (m/sec ²) Min/Max	Total time (sec)
Target 1	X	61309.3	54573.2	-2.95/-258.89	0/17.06	35
	Y	23646.12	17030.13	-289.59/-129.6	-16.45/0	
	Z	1258	1258	-1.49/3.56	-5.48/6.7	
Target 2	X	32783.37	32289.9	-149.29/14.08	-7.92/22.55	35
	Y	-40737.1	- 30199.25	265.78/304.86	-1.21/10.97	
	Z	4572	3843.8	-32.21/0.03	-12.19/0.6	
Target 3	X	60943.84	49353.21	-323.05/0	-1.2/3.77	55
	Y	60943.84	40374.41	-457.3/-323.05	-2.56/4.87	
	Z	3048	3048	-2.40/5.39	-7.9/7.3	
Target 4	X	30480	21159.82	-268.37/0	-36.57/53	80
	Y	9139.28	-7151.5	-275.05/229.05	-2.43/57.91	
	Z	2286	2286	-2.71/0.94	-8.53/3.65	
Target 5	X	80950.24	58057.3	0/-452.71	-32.3/66.44	80
	Y	969.75	16214.02	0/430.89	-46.9/67.05	
	Z	1448	1448	-0.45/1.4	-1.82/5.48	
Target 6	X	50351.19	49095.1	-287.79/0	-56.08/0	20
	Y	18499.28	10917.38	-426.7/-175.96	-10.3/51.81	
	Z	1548	807.64	-167.97/0	-67.05/48.7	

5.4 THE GENETIC ALGORITHM

Genetic algorithms are inspired by Darwin's theory about evolution. Solution to a problem solved by genetic algorithm is evolved [18].

Before describing algorithm, some biological terms used in the GA should be given for better understanding of the algorithm. All living organisms consist of cells which of each has the same set of *chromosomes*. A chromosome consists of *genes* and set of all chromosomes in organism is called *genome*. When two organisms are recombining (*crossover*), they share their genes and the resultant *offspring* may be mutated. Success of the organism shows the *fitness* of an organism.

The optimization process begins with initial population that is consisting of chromosomes. Chromosomes from population are taken according to their fitness and used to form a next population. Chromosome with more suitable fitness has more chances to reproduce. New chromosomes are produced in crossover and mutation phase. The resultant population is a combination of previous chromosomes and newly bred chromosomes. The cycle continues until the maximum number of population is reached. The algorithm can be summarized with the following steps:

1. Choose initial population
2. Evaluate the fitness of each chromosomes in the populations
3. Repeat
 - 3.1. Select best ranking chromosomes to reproduce
 - 3.2. Breed new generation through crossover and mutation and give birth to offspring
 - 3.3. Evaluate the individual fitnesses of the offsprings

- 3.4. Replace worst ranked part of population with offspring
4. Until reaching the maximum number of population

5.4.1 The Genetic Algorithm Toolbox

MATLAB GA tool is employed for optimization process. “ga”, command line function, applies the genetic algorithm to an optimization problem, using the parameters in the “option” structure created with “gaoptimset”. Parameter settings of “option” structure are given in Table 5-12. Other parameters of “option” structure, which are not mentioned in the table, are taken the default values. Further information about this toolbox can be found in MATLAB help document.

Table 5-12 Settings of MATLAB GA tool parameters.

<i>Parameter</i>	<i>Value</i>
Generations	50
Population size	15
Mutation Function	Uniform, with 0.1 rate
Elite Count	1
Crossover Fraction	0.7
Migration Fraction	0.05
Hybrid Function	FMINSEARCH

CHAPTER 6

RESULTS & DISCUSSION

Optimization of tracking radar simulator and RGPO models are performed over given scenarios in Chapter 5. As mentioned in the previous section, MATLAB GA tool is used for solving the associated optimization problems. MATLAB function 'fminsearch' is employed in order to improve the quality of the solution after terminating GA. This classical optimization algorithm uses the final point from the GA as its initial point.

In this chapter, the problem variables of tracking radar simulator are optimized and the results with the optimum parameters are discussed in section 6.1. Also, these optimum parameter values are used during the optimization of linear and parabolic RGPO variables over single target scenarios and the optimization results of RGPO models are given in section 6.2.

6.1 TRACKING RADAR SIMULATOR OPTIMIZATION

Tracking radar simulator optimization took approximately 48 hours for GA and nineteen hours for hybrid function with an Intel Centrino Core Duo

T2250 1.73 GHz processor. Results obtained are compared with the tracking radar simulator using default values of parameters. Defaults values, which are given in Chapter 5, are preferred for good comparison.

Minimum costs of each generation, which are obtained by using GA, are given in Figure 6-1.

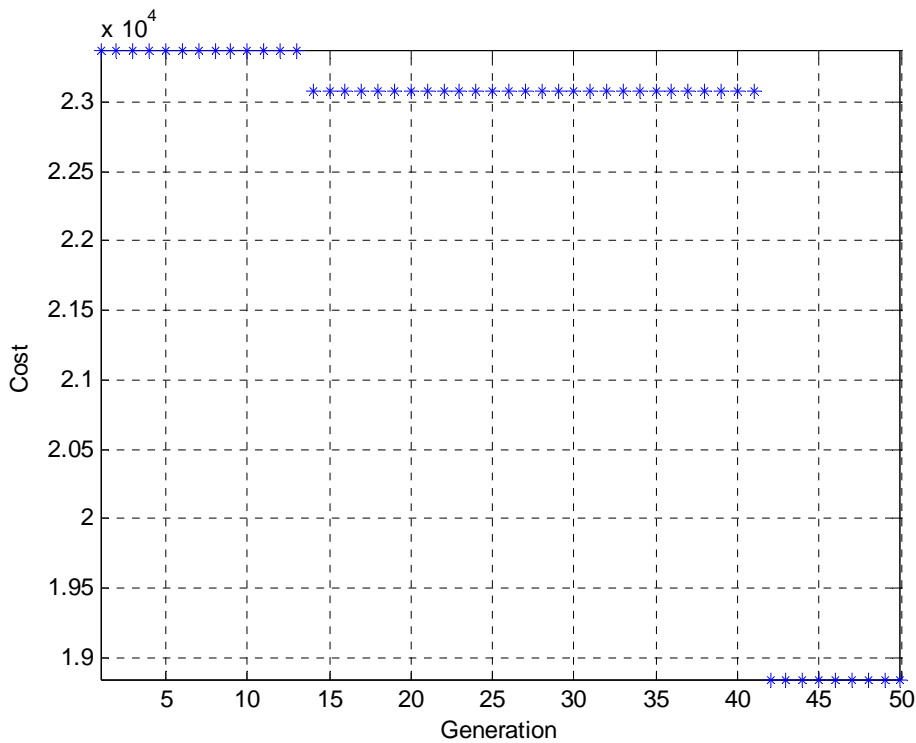


Figure 6-1 Costs of each generation for tracking radar simulator.

“fminsearch” function returns a better result because it decreases the last cost value of GA by 17%. Final results of the optimization are shown in Table 6-1.

Table 6-1 Optimized values of tracking radar simulator.

<i>Parameters</i>	<i>Optimized Value</i>	<i>Range</i>
Range gate width (m)	58.83	15-150
Probability of detection	0.71	0.5-1
Process noise standard deviation of CV model (m/sec ²)	48.86	1-50
Threshold for pruning	0.12	0.1-0.5
Confirmed target threshold	0.95	0.7-1

As seen from Table 6-1, range gate width is 58.83 meter, as expected; since small gate width yields successful tracking performance, especially for closely spaced targets. Gate width ranges are selected as 2 to 20 times of range resolution. On the other hand, the resultant value is 7.7 times of range resolution to allow tracking of fast targets.

Probability of detection is obtained as 0.71, which is not as high as expected. However, the higher the probability is, the less likely the algorithm will miss a real target but the more likely it will create a false target. As a result, this value is considered sufficient for our tracking radar simulator.

Optimum value of process noise standard deviation of CV model is acquired as 48.86 m/sec², which is relevant to $0.5 \times a_m \leq \sigma_v^2 \leq a_m$ where a_m is the maximum acceleration magnitude [25].

As shown in Table 6-1, pruning threshold is 0.12. This value is not as high as to be able to decrease the number of hypotheses significantly. Therefore, simulation took longer time than expected. In practice, pruning threshold is taken in between 0.1 and 0.5. This value can be selected in between 0 to 0.5 depending on the allocated simulation time, as smaller values yield more accurate results and higher values yield shorter simulation duration. Threshold for pruning higher than 0.5 will, obviously, yields to track loss.

Confirmed target threshold is obtained as 0.95, which is expected. The target is transferred to confirmed cluster if the probability equals to 1 [1].

Using these optimized values, all targets in multi-target scenarios are tracked successfully and no track loss occurs. Examples of these successful tracking are given in Figure 6-2, Figure 6-3 and Figure 6-4 for scenario 2, 4 and 6.

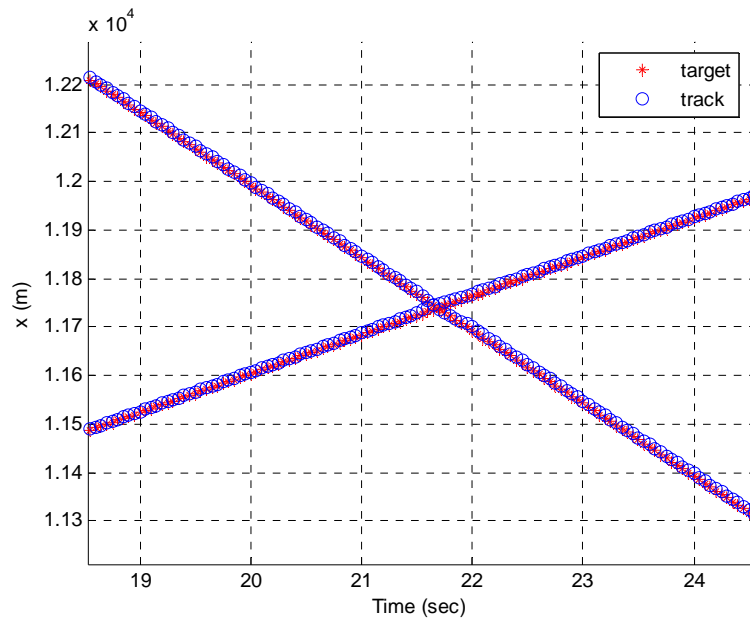


Figure 6-2 Target and track trajectories on the x coordinate for scenario 2 (crossing targets).

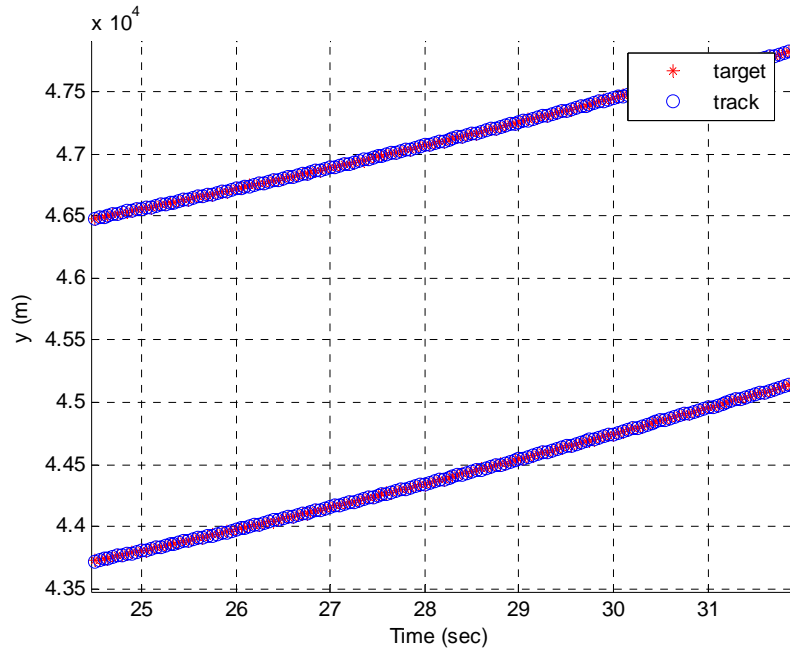


Figure 6-3 Target and track trajectories on the y coordinate for scenario 4 (parallel targets).

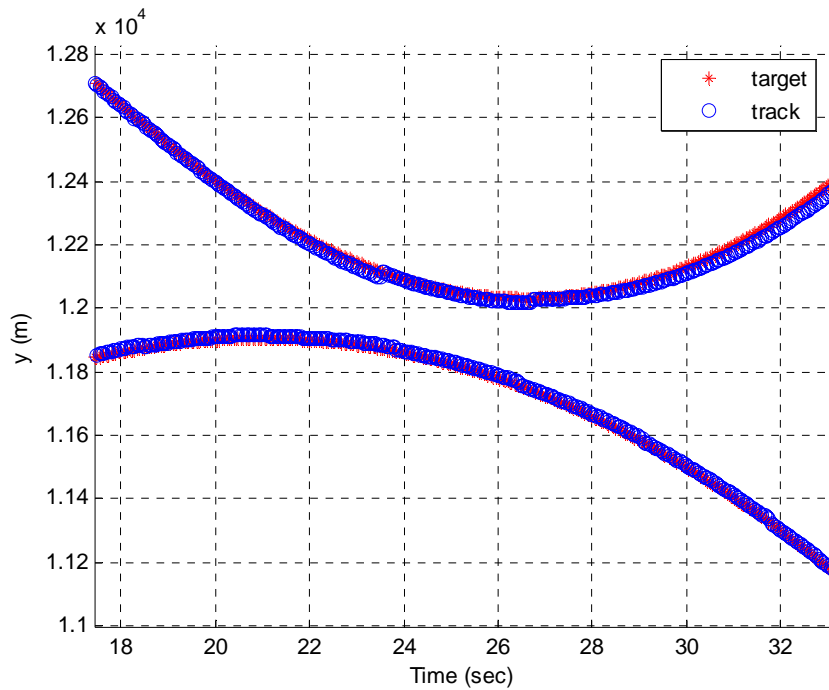


Figure 6-4 Target and track trajectories on the y coordinate for scenario 6 (converging-diverging targets).

Performances of tracking radar simulator with optimized values are given in Table 6-2, in which the number of scenarios, tracking error per dwell, false target tracking and track loss occurrences are presented, respectively. Almost all tracking errors are near to the range resolution value. These results indicate that tracking performance of our algorithm is successful. The reason that relatively higher values of tracking errors in scenario 7 have occurred may be the higher velocities of real target models.

Table 6-2 Performances of tracking radar simulator with optimized values.

<i>Scenario</i>	<i>TrackError/Dwell</i>	<i>False Track</i>	<i>Track Loss</i>
1	6.02, 8.12	No	No
2	8.5, 9.08	No	No
3	7.28, 7.66	No	No
4	6.53, 8.9	No	No
5	10.65, 7.75	No	No
6	10, 10.56	No	No
7	10.93, 12.98, 20.905, 15.456, 21.88, 27.65	No	No

As simulation runs using default values, it can be seen that, tracking radar simulator cannot track targets in scenarios 1, 2, 4 and 5. Therefore, track loss is occurred in all these scenarios. These unsuccessful trackings may have occurred due to higher default value of the track gate width.

On the other hand, targets in scenario 3 and 6 are successfully tracked. In scenario 7, track of target 1 is lost. Although the other targets of scenario 7 are tracked, tracking errors per dwell are higher than the values given in Table 6-2.

6.2 RGPO OPTIMIZATION

The main purpose of RGPO is to create a false target echo for stealing range gate of tracking radar and losing real target track. Therefore, the cost

function given in Chapter 5 is maximized for the optimization of RGPO parameters rather than minimizing for tracking radar simulator.

Performances of RGPO models will be evaluated over track loss. If the track is lost in each target of single target scenarios, RGPO technique is considered to be successful.

6.2.1 Linear RGPO

Almost three and half days run for GA with the same processor, maximum cost of each generation is obtained as given in Figure 6-5.

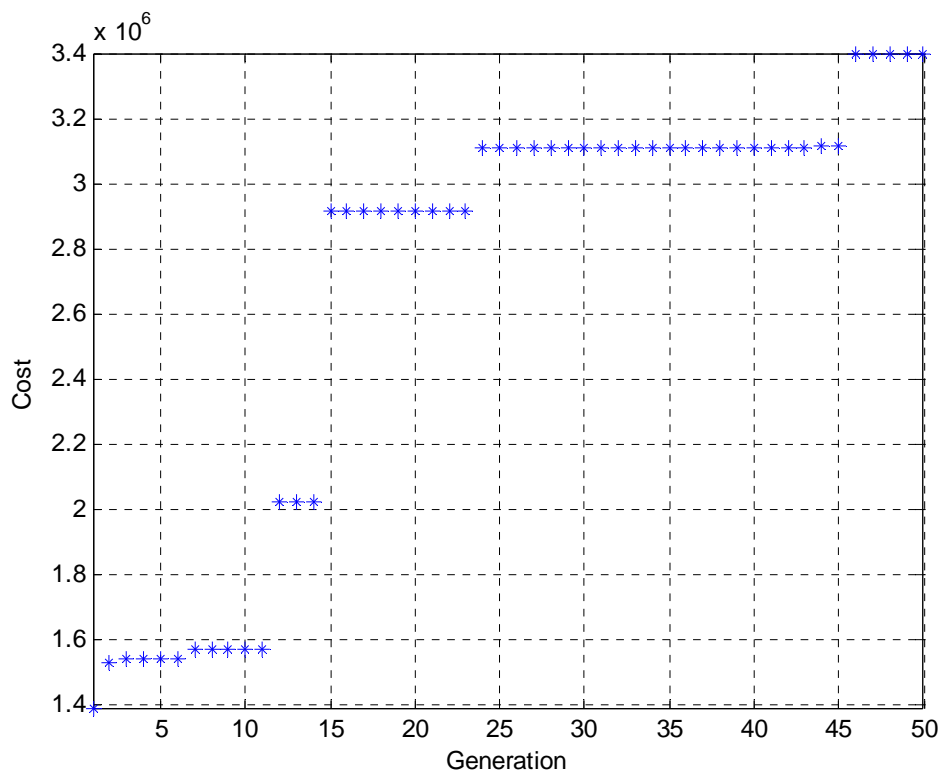


Figure 6-5 Costs of each generation for linear RGPO.

“fminsearch” function is not used for this optimization because it takes too much time and it does not improve the last cost value considerably. Optimization results of linear RGPO over single-target scenarios are shown in Table 6-3. When linear RGPO with these optimum parameters is used for each target in single-target scenarios, the range gate of tracking radar is successfully pulled off in all cases.

Table 6-3 Optimized values of linear RGPO.

<i>Parameters</i>	<i>Optimized Value</i>	<i>Range</i>
Rate (m/sec)	69.71	0-500
Initial reference time (sec)	12.82	10-50
End time (sec)	76.65	10-80
Amplification factor	3.07	1-4

As seen from Table 6-3, pull-off rate of linear RGPO is obtained as 60.71 m/sec. Range of this parameter is given between 0 and 500 since the largest single target velocity used for developing RGPO model does not exceed 500 m/sec.

Initial reference time and end time are acquired as 12.82 and 76.65 seconds, respectively. After the repeater pulse of RGPO captures the range gate of tracking radar, it moves the gate away from the target echo. At the same time of this occurrence, tracking error cost is increased. Therefore, optimum value of initial reference time is decreased as short as possible. On the contrary, end time is increased as long as possible.

Amplification factor is obtained as 3.07. Range of this value is taken from [14] between 1 and 4.

For instance; linear RGPO with optimum parameters is used for target 1 and 4 shown in Figure 6-6 and Figure 6-7.

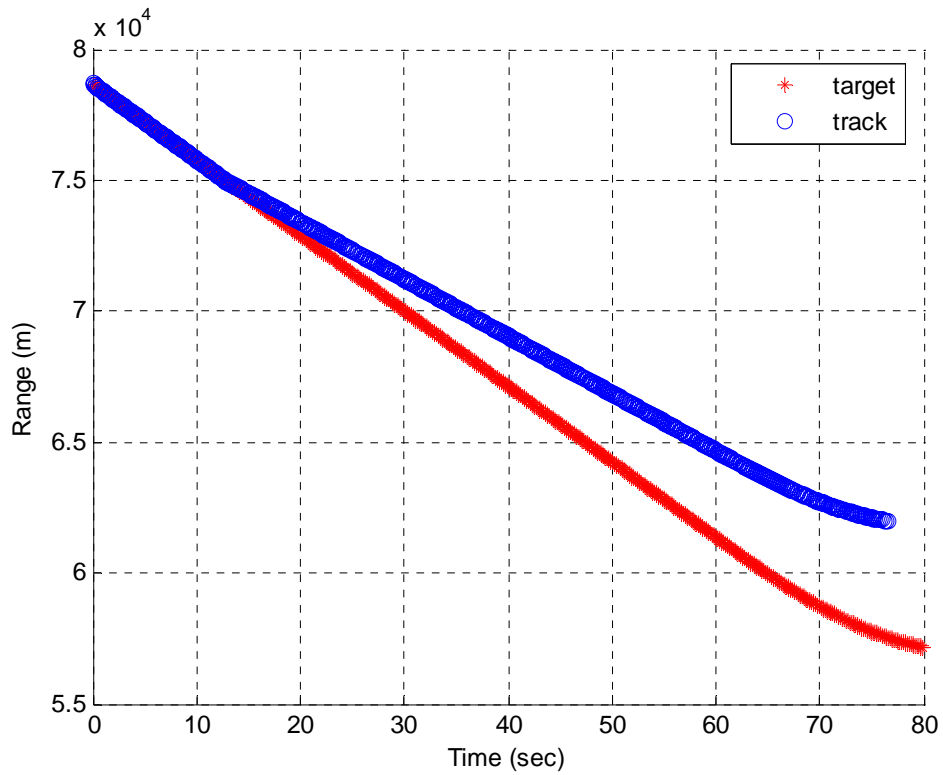


Figure 6-6 Output of linear RGPO for target 1.

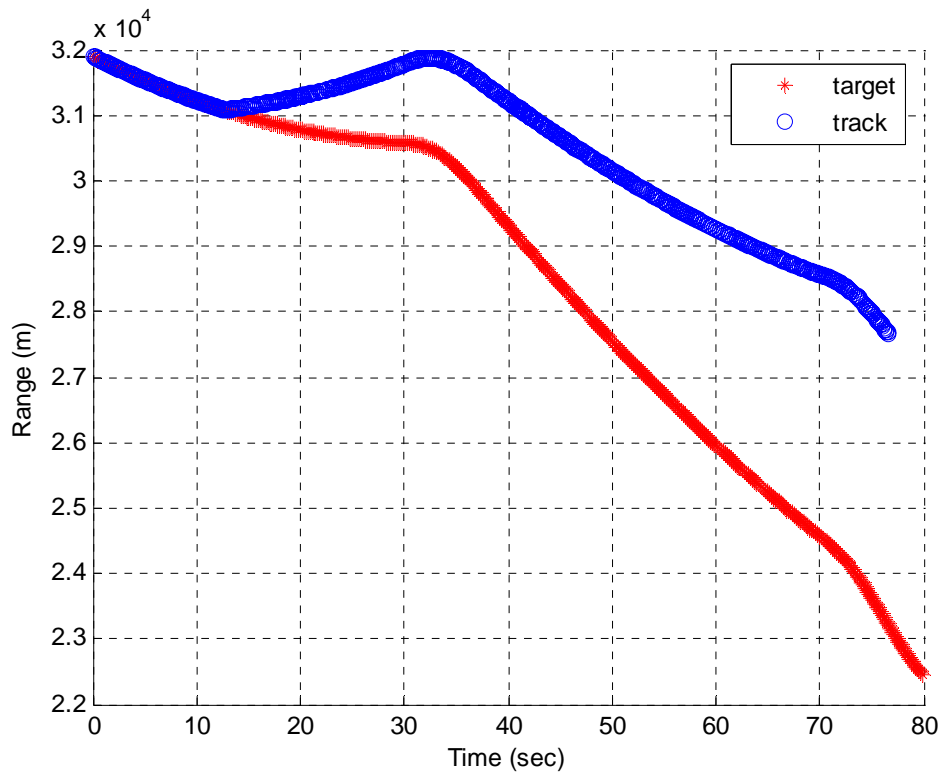


Figure 6-7 Output of linear RGPO for target 4.

6.2.2 Parabolic RGPO

Optimization of parabolic RGPO parameters took approximately three and a half days for GA with an Intel Centrino Core Duo T2250 1.73 GHz processor. Maximum costs of each generation are given in Figure 6-8.

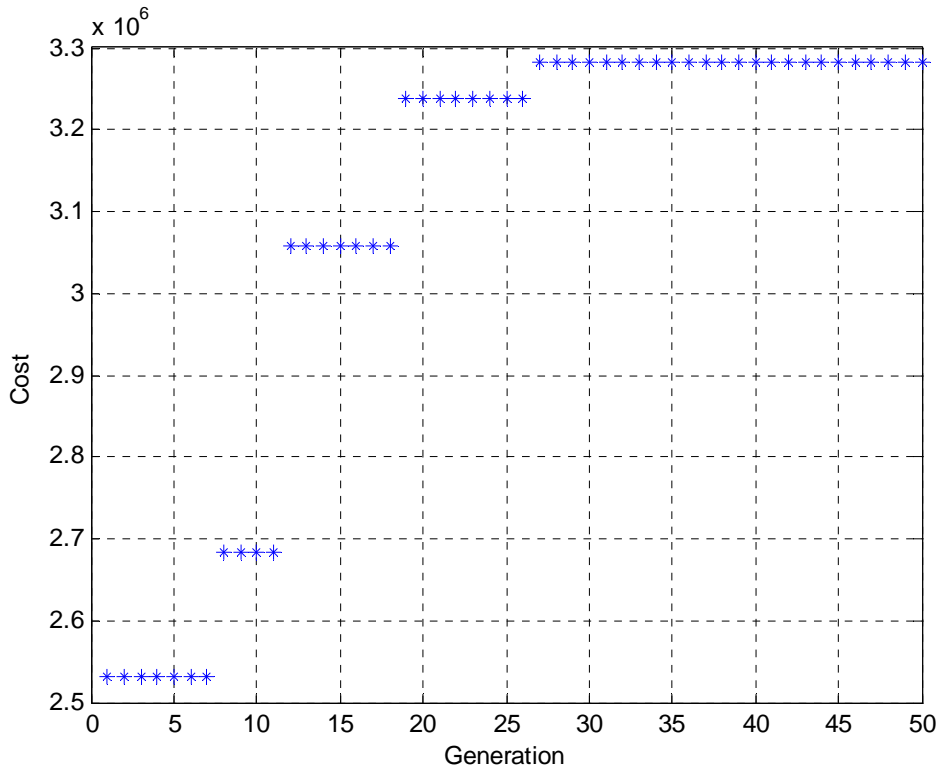


Figure 6-8 Costs of each generation for parabolic RGPO.

“fminsearch” function is not used either for the optimization of parabolic RGPO model. The optimized values of GA output are shown in Table 6-4.

Table 6-4 Optimized values of parabolic RGPO.

<i>Parameters</i>	<i>Optimized Value</i>	<i>Range</i>
Acceleration (m/sec ²)	14.35	0-80
Initial reference time (sec)	17.06	10-50
End time (sec)	78.96	10-80
Amplification factor	3.21	1-4

As shown in the table above, acceleration parameter of parabolic RGPO is obtained as 14.35 m/sec^2 . Range of this parameter is given in between 0 and 80 since the largest single target acceleration used for developing RGPO model does not exceed 80 m/sec^2 .

Initial reference time and end time are acquired as 17.06 and 78.96 seconds, respectively. Optimum value of the end time is long enough, and, on the other hand initial reference time is short enough to increase the tracking error cost, when the RGPO steals the range gate of the tracking radar.

When the parabolic RGPO with optimum parameters is used for target 3 and 5, the range of false targets are shown in Figure 6-9 and Figure 6-10, respectively.

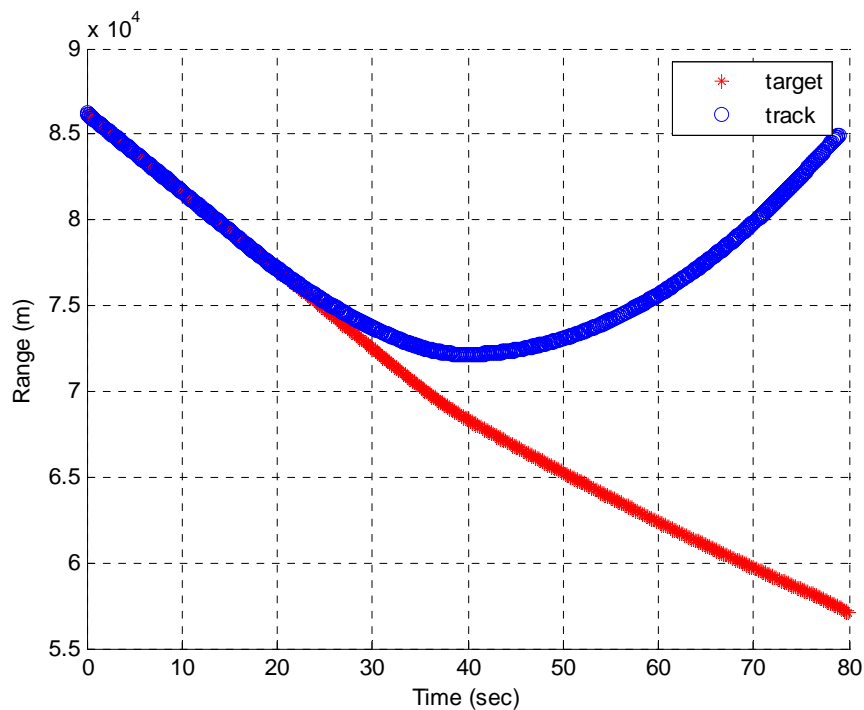


Figure 6-9 Output of parabolic RGPO for target 3.

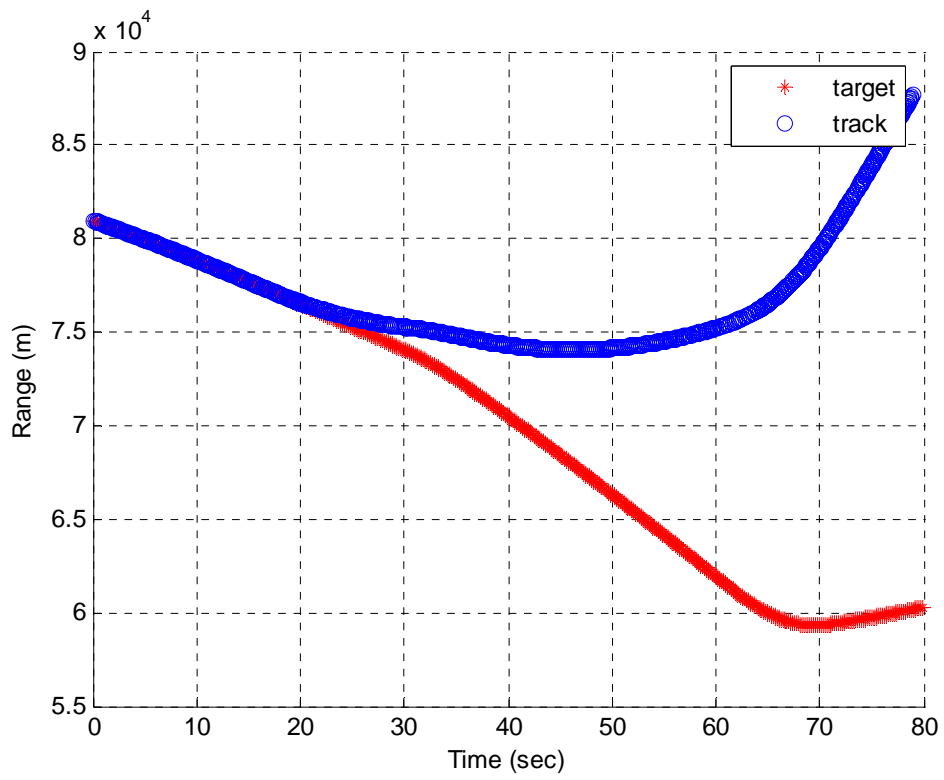


Figure 6-10 Output of parabolic RGPO for target 5.

CHAPTER 7

CONCLUSION

The aim of thesis is to develop EA and tracking system and also to optimize the performances of these systems.

Tracking radar simulator, which consists of a monopulse tracking radar and an MHT tracker, is implemented, since monopulse tracking radar is not effected from target scintillation and angle of target is measured more precisely than the other methods. In addition, MHT is widely accepted to be the most successful data association algorithm and also it performs better than the other tracking algorithms such as IMMJPDA.

EA presents a greater challenge to target tracking compared to clutter and missed detections. Primary technique of EA against tracking radar is RGPO which is also chosen to be optimized. RGPO is modelled as two modes: linear and parabolic.

Simulator environment is implemented in MATLAB software depending on a monopulse tracking radar, an MHT tracker, target models and RGPO

model principles. Cost function is constructed including tracking error, false target and target loss costs. This cost function output is used as an input for the MATLAB GA tool in the optimization problem of both the tracking radar and the RGPO model.

Tracking radar simulator is improved by the optimization of its parameters for achieving best tracking capability. Optimization is performed over all multi-target scenarios since suitable parameter values are required for generalized scenarios. Multi-target scenarios are prepared by considering extreme cases (target models). Also, real target motions are input for the last scenario to assess the performance of the tracking radar on real target cases. Results obtained at the end of the tracking radar optimization indicate that all targets in multi-target scenarios are tracked successfully even for the extreme cases. No track loss has occurred for all targets but relatively larger tracking errors are encountered in real target cases. Thus, we can conclude that a successful tracking radar simulator is improved.

RGPO technique is developed to improve the effectiveness against this tracking system. Both linear and parabolic RGPO parameters are optimized in this study. Optimization is performed over all single-target scenarios consisting of real target models since suitable parameter values are required for generalized target cases. Both linear and parabolic RGPO models are observed as successful pull-off the range gate of the tracking radar even though real target models are used.

To conclude, this work shows that successful tracking is achieved by a tracking system with a monopulse tracking radar and an MHT tracker. In addition, finding the optimum parameters of EA system is guaranteed to deceive the victim radar under used target models. This thesis indicates the importance of developing EA systems and other types of EA can be developed by similar approaches in the future. This study is considered truly beneficial for our country as well as the international community (since there is limited study available in the field of developing of EA systems, mainly because of confidentiality).

REFERENCES

- [1] Reid, D. B., "An Algorithm for Tracking Multiple Targets", IEEE Transactions on Military Electronics, Vol. AC-24, No. 6, December 1979.
- [2] Blackman, S., Popoli, R., "Design and Analysis of Modern Tracking Systems", Artech House, Inc., 1999.
- [3] Blackman, S., "Multiple Hypothesis Tracking for Multiple Target Tracking", IEEE A&E Systems Magazine, Vol. 19, No. 1, January 2004.
- [4] Şahin, M.A., "Performance Optimization of Monopulse Tracking Radar", M.Sc. Thesis, 2004.
- [5] Bar-Shalom, Y., Li, X., "Multitarget-Multisensor Tracking: Principles Techniques", 1995.
- [6] Bar-Shalom, Y., Tse, E., "Tracking in a Cluttered Environment with Probabilistic Data Association", Automatica, Vol. 11, Pages: 451-460, 1975.
- [7] Bar-Shalom, Y., "Extension of the Probabilistic Data Association Filter in Multi-Target Tracking", in Proc. 5th Symp. on Nonlinear Estimation, Pages: 16-21, September 1974.
- [8] Lundin, K., "A System for Analysis of Human Pain Signals Using a Radar Tracking Approach", Department of Clinical Neurophysiology, Uppsala University, October 1998.
- [9] Blackman, S., "Multiple-Target Tracking with Radar Applications", Artech House, Inc., 1986.

- [10] Barton, D.K., Leonov, S. A., "Radar Technology Encyclopedia (Electronic Edition)", Artech House, Inc., 1998.
- [11] Rhodes, D.R. "Introduction to Monopulse", Artech House, Inc., 1980.
- [12] Skolnik, M., "Radar Handbook", McGraw Hill Inc., 1990.
- [13] Blair, W.D., Watson, G.A., Hoffman, S.A., Gentry, G.L. "Benchmark Problem for Beam Pointing Control of Phased Array Radar Against Maneuvering Targets in the Presence of ECM and False Alarms", Code B32 System Research and Technology Department Naval Surface Warfare Center/ Dahlgren Division, February 1995.
- [14] Blair, W.D., Watson, G.A., Kirubarajan, T., Bar-Shalom, Y. "Benchmark for Radar Allocation and Tracking in ECM", IEEE Transactions on Aerospace and Electronic Systems, Vol. 34, No. 4, October 1998.
- [15] Nerri, F., "Introduction to Electronic Defense Systems", Artech House, Inc., 2001.
- [16] Van Brunt, L.B., "Applied ECM Volume 1", Ew Engineering, Inc., 1978.
- [17] Farina, A., Miglioli, R., Graziano, A., de Feo, M., "IMMJPDA versus MHT and Kalman Filter with NN Correlation: Performance Comparison", IEEE Proc.-Radar, Sonar Navig., Vol. 144, No. 2, April 1997.
- [18] <http://cs.felk.cvut.cz/~xobitko/ga>
- [19] Rui, Z., Zhang, J., Jigang, Z., Wenxiu, L. "Laser Target Tracking Based on Converted Measurement Kalman Filter", Proceedings of the Fourth World Congress on Intelligent Control and Automation, June 2002.

- [20] Van Trees, H.L., "Optimum Array Processing", John Wiley & Sons, Inc., 2002.
- [21] Schlosser, M.S., Kroschel K. "Limits in Tracking with Extended Kalman Filters", IEEE Transactions on Aerospace and Electronic Systems, Vol. 40, No. 4, October 2004.
- [22] Schleher, D.C., "Introduction to Electronic Warfare", Norwood, MA: Artech House, 1986.
- [23] Streetly, M., "Jane's Radar and Electronic Warfare Systems", 11th edition, 1999-2000.
- [24] Fortmann, T. E., Bar-Shalom, Y., Scheffe, M., "Sonar Tracking of Multiple Targets Using Joint Probabilistic Data Association", IEEE Journal of Oceanic Engineering, OE-8, Pages: 173-184, July 1983.
- [25] Bar-Shalom, Y., Li, X., Kirubarajan, T., "Estimation with Applications to Tracking and Navigation", John Wiley & Sons, Inc., 2001.
- [26] Rong Li, X., Slocumb, B., West, P., "Tracking in the Presence of Range Deception ECM and Clutter by Decomposition and Fusion", Proc. SPIE, Vol. 3809, Pages: 198-210, 1999.